Perovskite Nanostructures: leveraging quantum effects to challenge optoelectronic limits

Sneha A. Kulkarni,[a] Natalia Yantara,[a] Kim Seng Tan,[a] Nripan Mathews,*[a,b] Subodh G. Mhaisalkar,*[a,b]

[a.]Energy Research Institute at Nanyang Technological University (ERI@N), Research Techno Plaza, X-Frontier Block, Level 5, 50 Nanyang Drive, Singapore 637553, Singapore.

[b.]School of Materials Science and Engineering, Nanyang Technological University, Nanyang Avenue, 639798, Singapore.

Email: Nripan@ntu.edu.sg; Subodh@ntu.edu.sg

Abstract

Metal halide perovskites have affirmed their pedigree as extraordinary semiconducting materials, exhibiting properties rivalling those observed in single crystal compound semiconductors. Perovskites show tremendous versatilities in both structure and composition tuning, and therefore applications ranging from optoelectronics to X-ray imaging and spintronics, neuromorphic electronics are emerging. Moreover, when their dimensions become comparable to the exciton Bohr radius, perovskite nanostructures and layered systems display remarkable properties because of quantum confinement. Nanostructured and lower dimensional layered perovskites exhibit properties that are yet to be fully exploited such as extraordinarily high luminescence, narrow emissions, high exciton binding energies, strong non-linear phenomena, and carrier cascade characteristics. This review, while highlighting the frontier phenomena that continue to be unravelled, outlines how confined structures of these materials have demonstrated properties that promise to unlock exceptional quantum phenomena to challenge the optoelectronic limits.

Keywords: Perovskite nanostructures, quantum confinement, dimensionality, optoelectronics, photovoltaics

1. Introduction

Metal halide perovskites have revolutionized the practice of using solution processed materials for solar cell and light-emitting device applications. They possess exceptional intrinsic properties such as defect tolerant, large optical absorption coefficient, long carrier diffusion lengths, crystalline nature, and tunable binding energies (E_b) [1, 2]. Within ten years, perovskite-based solar cells have grown rapidly with efficiencies reaching 25.2%, representing the highest efficiency of any solution-processed device[3]. Halide perovskites have also proven their existence in other optoelectronic applications such as light emitting devices, where external quantum efficiencies (EQE) of perovskite-based light emitting diodes (PeLED) have evolved from below 1% to more than 20% in 5 years; making them highly potential for large area lighting and display applications [4, 5]. Moreover, low amplified spontaneous emission (ASE) thresholds in cavity-free formations have revealed the relevance of these materials as gain medium for lasing applications [6]. In general, the key to the successful deployment of halide perovskites for numerous optoelectronic applications lies in the ability to modify the materials' optoelectronic properties via tailoring the perovskite compositions and structures to reduce non-radiative recombination.

Earlier studies in solar cells and LEDs have been focused on AMX_3 perovskite with a three-dimensional (3D) inorganic octahedral [MX_6] structural framework, wherein A, M, X represent monovalent cation [e.g. Cs^+, methylammonium ($CH_3NH_3^+$ = MA^+), formamidinium ($HC(NH_2)_2^+$ = FA^+)], metal ion (e.g. Pb^{2+}, Sn^{2+}, Ge^{2+}), and an anion (e.g. I^-, Br^-, Cl^-) respectively (**Figure 1a**) [7, 8]. Apart from the 3D structure, additional alternatives are also represented by lower–dimensional layered structures which are formed by the incorporation of larger cations (A^+) in the 3D structure. This leads to the reconstruction of the AMX_3 framework into 2D-3D, mixed dimensional perovskite structures, also known as 'quasi-2D' structures. The quasi 2D variants are defined in terms of (n), which represent the number of connecting inorganic octahedral structures present between two bulky cations layers. Depending on the choice of the A^+, two types of quasi 2D structures can be formed, i.e. the Ruddlesden-Popper (RP) and the Dion−Jacobson (DJ). In typical RP perovskites ($A'_2A_{n-1}M_nX_{3n+1,}$ A' = +1), the unit cell (n = 1, A'_2MX_4) is formed by inserting a pair of monovalent organic cation 'A″' (e.g. benzyl ammonium (BZA), phenylethyl ammonium (PEA), octylammonium (OA)) in between the inorganic octahedral layers. Whereas, in the DJ phase ($A''A_{n-1}M_nX_{3n+1,}$ A' = 2+), the unit cell (n = 1, $A''MX_4$) is formed by incorporating a single layer of either divalent organic cation 'A′' (e.g. 3-(aminomethyl) piperidinium (3AMP) or 4-(aminomethyl) piperidinium

(4AMP))[9] or the diammonium cation (e.g.1,4-Benzenedimethanamonium)[10] (**Figure 1b**). As the optoelectronic properties are tied closely with the perovskite crystal structure, fine tuning the choice of the cations and the amounts of A and A′ cations will lead to a range of quasi 2D perovskites with vastly diversified optical and electronic properties which can be harnessed to tailor the properties to meet specific needs. For example, significantly differing dielectric constants between organic and inorganic layers can be harnessed to aggravate dielectric confinement which engenders significant enhancement in PeLED as well as lasing attributes [11-13]. In response, solution processed RP microplates have demonstrated highly stable and low lasing threshold down to 7.8 μJ cm^{-2} attributed to enhanced exciton and photon confinement in RP structures [14].

Another strategy to regulate the optoelectronic properties is by utilizing perovskite nanostructures. Nanostructures of different morphologies and spatial dimensionalities (e.g. nanoparticles, quantum dots (QDs), nanorods (NRs), nanowires (NWs), and nanoplatelets (NPLs)) can be synthesized (**Figure 1c**) [4, 15-19] by judiciously controlling the reaction parameters. They exhibit fascinating physical properties due to either quantum confinement or strong anisotropy, and display high PLQY (~ 100 %), narrow emission, size and shape dependent colour tunability and other striking attributes which are comparable or exceed the metrics of inorganic semiconductor QDs (e.g. CdSe) [17, 20-22] Perovskite nanocrystals (NCs) have recently been shown to yield high performance solar cells [15], exhibit slow hot-carrier cooling [23], as well as efficient multi-exciton generation (MEG) [24, 25]. Charge carrier cascade in nanoparticle assemblies has also yielded high performance LEDs [26], whereas core-shell NCs have displayed large multiphoton absorption cross-sections [27, 28]. Perovskite NWs and NPLs with strong optical and dielectric confinement have shown promise for photonics (e.g. lasers) applications due to their composition and structure driven tuning of photophysical properties [29-31].

Both nanostructured and layered perovskites leverage confinement effects to yield high performance LEDs, slow-hot carrier cooling, multi exciton generation, low-threshold polarized lasing, and impressive non-linear properties. These phenomena made available by quantum effects promise to enable new materials and device structures that will enable us to challenge the Shockley Queisser (SQ) limit, yield high performance light emitting devices and lasers. This review, while highlighting the materials attributes driving these advances, will also discuss related frontier phenomena that are being uncovered in these versatile perovskite nanostructures.

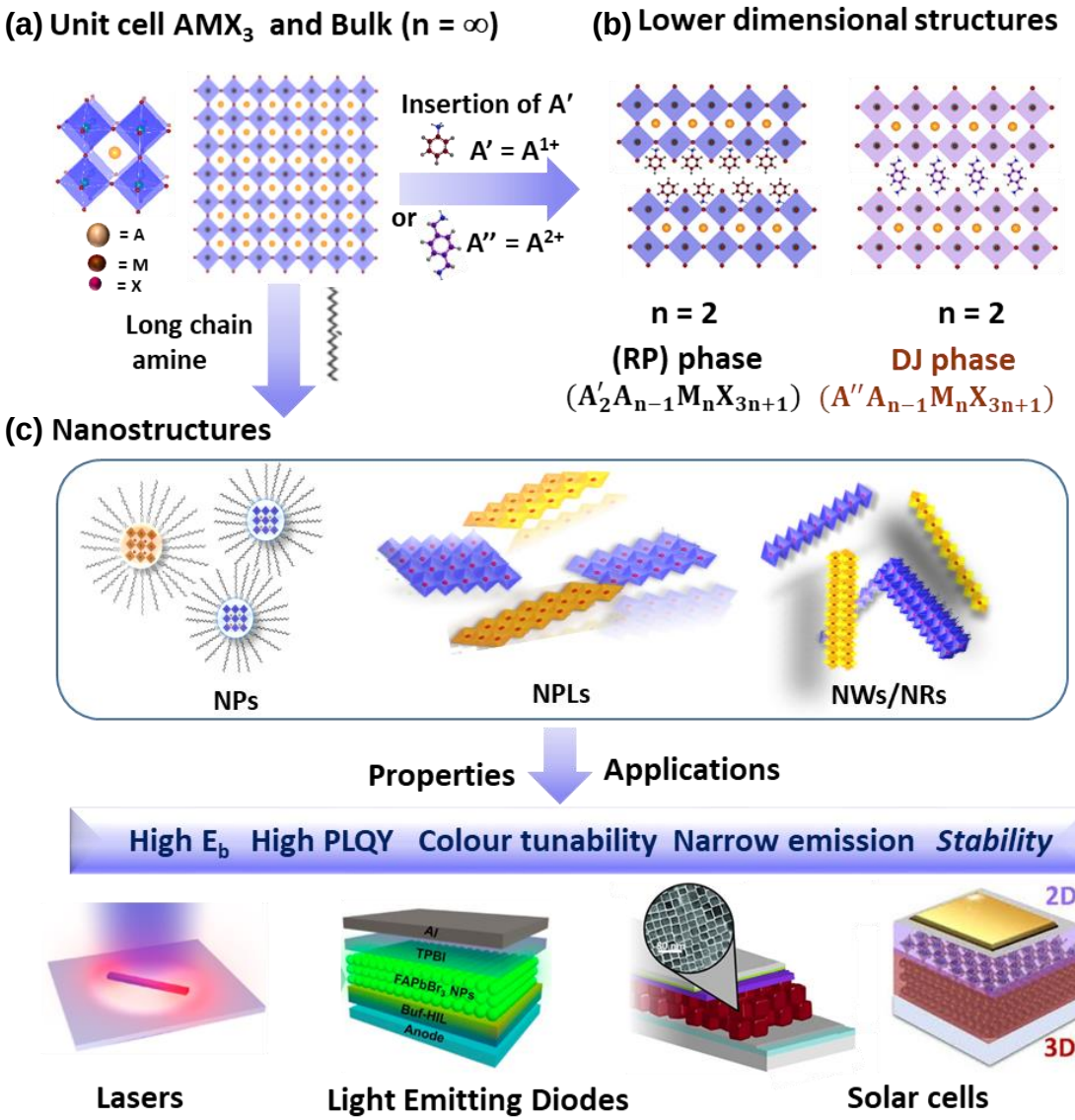

Figure 1: *Schematic illustration of (a) AMX_3 type unit cell of 3D perovskite together with (b) lower–dimensional layered perovskites phases, e.g. RP perovskites and DJ with n=2 phases. (c) Perovskite nanostructures such as NPs, NRs, NWs, and NPLs along with their unique properties and potential application in various fields of optoelectronic, reprinted with permission from* [15, 16, 30, 32, 33].

2. Influence of confinement on the photophysical properties of perovskites

The relationship between the perovskite composition and structure to the photo physical properties of the halide perovskites will be reviewed herein from the electronic band structure, carrier dynamics, and recombination dynamics point of view. Synthesis route and crystal structure stability of chemically modified perovskites, as governed by the Goldschmidt and octahedral factors, have been well reported elsewhere in the literature [34, 35].

2.1 Electronic band structure modulation

Density Functional Theory (DFT) analyses have indicated that the electronic band structure near the band edges is primarily influenced by the [MX_6] octahedra [36, 37]. In $MAPbI_3$, the valence band maximum (VBM) comprises antibonding states from the hybridization of Pb 6s and I 5p orbitals, whereas the conduction band minimum (CBM) is formed by empty Pb 6p orbitals with secondary contribution from I 5s orbitals [36]. This band structure induces the defect tolerant nature of the perovskites as the defect energy levels lie either within the conduction or valence band (**Figure 2a**) [17]. A high absorption coefficient is observed as the p orbitals (which have less dispersion than s orbitals) govern the band edge and consequently yield high joint density of states (JDOS) at the band edge [38]. Whereas, the small stoke shift in photoluminescence (PL) spectra is indicative of electron – hole recombination from CBM to VBM [39]. Halide substitution results in a shift in the VBM, leading to a reduction in E_g for larger atomic sizes (Cl → Br → I), which can be predicted by Vegard's law [40].

On the other hand, substitution of Pb with smaller Sn cation results in the reduction of the E_g to ~1.3 eV for $MASnI_3$ [41]; attributed to the spin-orbit coupling (SOC) effect that splits the states near CBM [39]. Anomalous bandgap changes observed for Pb – Sn perovskites (where the lowest bandgap was found in the mixed $MASn_{0.5}Pb_{0.5}I_3$ system rather than $MASnI_3$) are speculated to be caused by similar orbital composition between CBM and VBM of $MASnI_3$ and $MAPbI_3$, analogous to the $Pb_{1-x}Sn_xTe$ system [41]. Although the 'A' cation seems to play a minor role in the perovskite band structure, the choice of the A cation modulates the M – X bond angle or the [MX_6] octahedral dimensionality that subsequently alters E_g. Decreasing the [MX_6] octahedral tilt by employing FA cations that promote hydrogen bond formation with inorganic matrix enhances the metal p contribution in the CBM, resulting in an increased spin-orbit splitting and a reduction in E_g [37]. Employing smaller cations (such as Cs^+) reduces the M – X – M bond angle causing a linear increase in E_g [42]. In practice, multi-cation approaches by mixing FA, MA, and Cs for example, that have been used to stabilize the perovskite structure [43] can also modulate the M – X – M bond angle and E_g. Addition of bulky organic molecules at the A site (as in RP perovskites) leads to a reduction of the [MX_6] octahedral dimensionality to form a layered octahedral framework that shrinks the bandwidth of both CBM and VBM and increases the E_g of the material [39]. Steric effects influenced by cation shape and size[42, 44], electrostatic attraction related to charge state of the cation [9], and the position of the functional group play a role in influencing the [MX_6] inorganic octahedral slabs. An E_g value of ~ 2.43 eV was obtained when long alkyl chain amine derivative such as n-

butylamine ($C_4H_9NH_3$) was used to form the $(C_4H_9NH_3)_2PbI_4$ layered perovskite structure with a sharp optical absorption onset indicating direct bandgap properties [38]. Longer alkyl chain molecules, such as $C_6H_{13}NH_3$ and $C_{12}H_{25}NH_3$ can also be incorporated resulting in E_g values of 2.7 eV and 2.88 eV respectively[45].

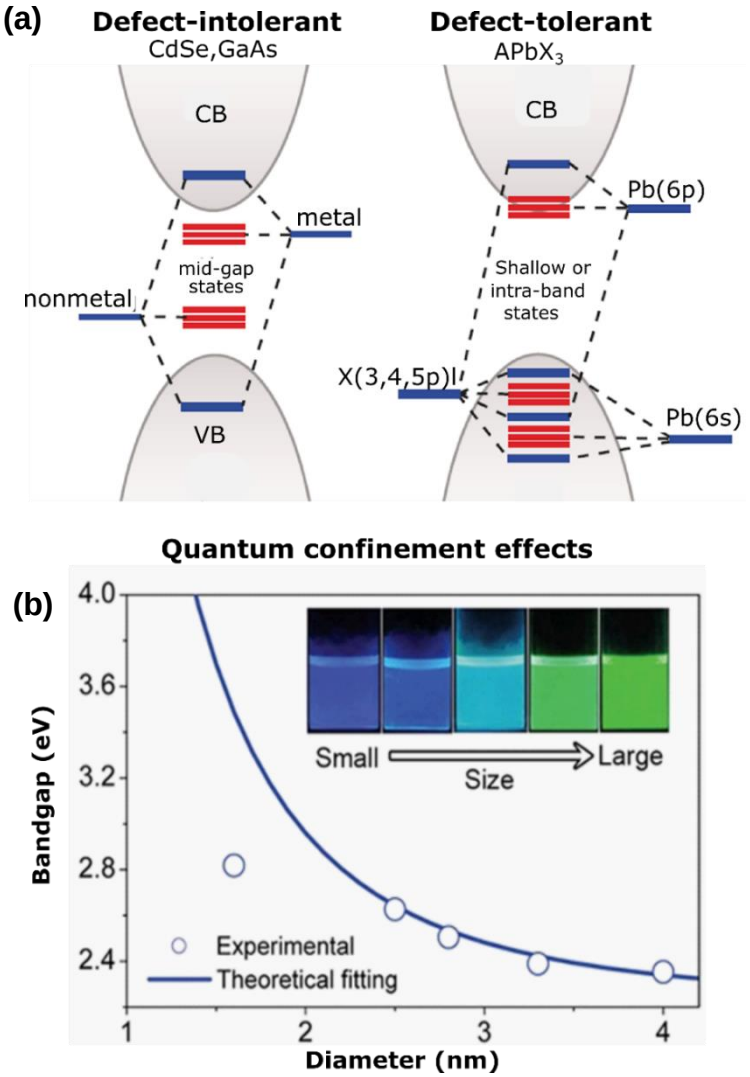

Figure 2: *(a) Schematic diagram of electronic structures comparing defect tolerance and defect intolerant system, reprinted with permission from [17]. (b) Experimental and theoretical bandgap modulation of $MAPbBr_3$ nanocrystals with size reduction. Reprinted with permission from [46].*

Further fine-tuning of the E_g can be done by varying the numbers of inorganic octahedral layers in between the bulky molecules (n). Modification of E_g in the range of 2.43 eV to 1.5 eV with increasing octahedral layers (n) value has been reported in the $(C_4H_9NH_3)_2(MA)_nPb_nI_{3n+1}$ system [38]. The use of bulky organic cations results in the formation of multi quantum well like structures with low dielectric constant (ε) organic molecules and high ε inorganic layers,

creating a dielectric confinement effect inside the lower dimensional perovskites (i.e. 2D and 1D) [34]. Consequently, these layered structures effectively confine excitons and enhance radiative recombination probability (refer to **sections 2.2 and 2.3).**

In nanostructures, as the dimension of the material approaches the Bohr radius (r_b), discrete electronic structures are formed leading to an increase in E_g (called quantum confinement). Size-induced quantum effects were demonstrated in $CsPbBr_3$ nanocrystals, with a blue shift (2.42 eV nm to 2.67 nm) was observed with the reduction in size from 11.8 nm to 3.8 nm [47]. Blue shifts in the range of (~0.4 – 0.5 eV were observed in $MAPbBr_3$ NPLs and NCs with thickness reduction from 3 nm to 0.6 nm and a reduction in diameter from 3.9 to 1.6 nm respectively (**Figure 2b**) [46]. Although high surface area nanocrystals will lead to an increase in surface defects, due to their defect tolerance nature, surface traps in the perovskites NCs are relatively benign and do not perturb the optical and electrical properties significantly even without a complex surface passivation technique. Nanocrystals with PL efficiency close to 100% have been realized even without surface passivation. Nanocrystals with PL efficiency close to 100% have been realized [48], thus highlighting the impact of nanostructuring on perovskites.

2.2 Charge Carrier Dynamics

Techniques such as magneto absorption spectroscopy, temperature dependent photoluminescence (PL), and optical absorption studies have been employed to measure the strength of Coulombic attraction between electrons – hole pairs (i.e. E_b) and to investigate the excitonic versus free carrier nature of charges generated in perovskites. Magnetoabsorption spectroscopy revealed that E_b of $MAPbI_3$ ranges from 37 meV to 50 meV dependent on the choice of dielectric function (ε) [49, 50]. With PL intensity decreasing with rising temperatures, temperature dependent PL spectroscopy indicated exciton dissociation, with E_b values ranging from 19 meV to 62 meV [51, 52]. Elliot's theory [53] of band onset absorption was also utilised to estimate E_b, with values ranging from 5 to 25 meV[54, 55].

At room temperature, thermal energy (k_bT_{298K}), will dissociate excitons, which will create free carriers as the primary carrier population for $MAPbI_3$. Photoinduced terahertz conductivity, PL and transient absorption (TA) spectroscopy measurements have confirmed the presence of free carriers as the primary photogenerated species [56, 57]. The generation of free carriers in 3D perovskites facilitates charge extraction for photovoltaic applications. As E_b values are

inversely proportional to the dielectric constant ($E_b \propto {}^{1}/_{\varepsilon^2}$) and exciton Bohr radius (r_b) is proportional to dielectric constant ($r_b \propto \varepsilon$) of the materials, the E_b and r_b values can be varied by introducing low dielectric constant organic molecules in the system.

While Mott-Wannier model describes systems with low E_b (E_b ~ 10 meV) with Bohr radii much larger than that of the host lattice (r_b >> a) (**Figure 3a)**, Frenkel excitons represent a system with tightly bound excitons ($E_b \geq \sim$ 100 meV) with small Bohr radii ($r_b \leq$ a). Therefore, depending on the choice of organic molecules and the inorganic octahedral layer thickness in between the layers of bulky organic molecules present in the system, excitons generated in halide perovskites can be classified as Mott-Wannier excitons or Frenkel excitons. E_b values above 100 meV have been observed in layered perovskites depending on the choice of the bulky organic molecules, its dielectric constant and its interaction with the [BX_6] inorganic octahedral slab. Long alkyl chain molecules such as $C_{10}H_{21}NH_3^+$ can be employed to boost the E_b to 320 meV [58], whereas fluorinated aromatic molecules (e.g. 4-$FC_6H_4C_2H_4NH_3^+$) can increase the E_b to 540 meV[45]. The enhancement on the E_b has been attributed to both the use of low dielectric constant organic molecules and dielectric confinement effect found naturally in the layered perovskite structure (**Figure 3b**) [59-62], with E_b shown to vary with the ratio of dielectric constants of both inorganic and organic layers [59, 62]. Partial substitution with bulky organic molecules would lead to quasi-2D materials, with decreasing octahedral inorganic layers resulting in E_b enhancement. E_b value of 170 meV were reported for $(C_6H_4C_2H_4NH_3)_2(MA)Pb_2I_7$ with n = 2 layers as opposed to 220 meV for n = 1 compounds [51]. Similar effects were also observed with long alkyl chain molecules, where $(C_4H_9NH_3)_2PbI_4$ compounds with variations in n from 1 to 3 resulted in E_b values of 290 meV and 150 meV respectively [62].

The nature of excitons for 2D perovskites is still an open question, with reports of Wannier excitons in the inorganic matrix and the presence of small radii Frenkel excitons in the organic framework [63]. Variations in the organic cations and inorganic layers modulated both E_b and r_b, which add to the complexity in the assignment of the excitons' nature [34]. Interestingly, the possibility of the formation of Frenkel-Wannier hybrid excitons had been reported [34]. Properties of these hybrid excitons result from contributions of optical nonlinearity and large oscillator strength of Wannier and Frenkel excitons respectively [64]. These hybridized properties can be gainfully exploited in light emitting diodes, lasers, and nonlinear optics (i.e. second and third harmonic generation). In perovskite nanocrystals, both size and organic (surface) ligands confinement confine electron-hole pairs within the particles (**Figure 3b**).

These confinement strategies would increase the E_b of the materials, which subsequently shift the nature of carriers to be dominated by tightly bound Frenkel excitons[65-67]. Strong carrier confinement in 3.4 nm $CsPbBr_3$ NPLs have been reported, which lead to E_b 120 meV, as opposed to value of ~ 33 meV in $CsPbBr_3$ thin film[68]. Quantum confinement effects were also observed in $MAPbBr_3$ NCs and NPLs with E_b ranging from 320 meV to 600 meV, influenced by nanoplatelet thickness [67, 69]. Layered perovskites in nanostructured form, e.g. NSs of $(C_4H_9NH_3)_2PbI_4$ result in E_b of 490 meV [70] as opposed to 290 meV for its bulk counterpart [62].

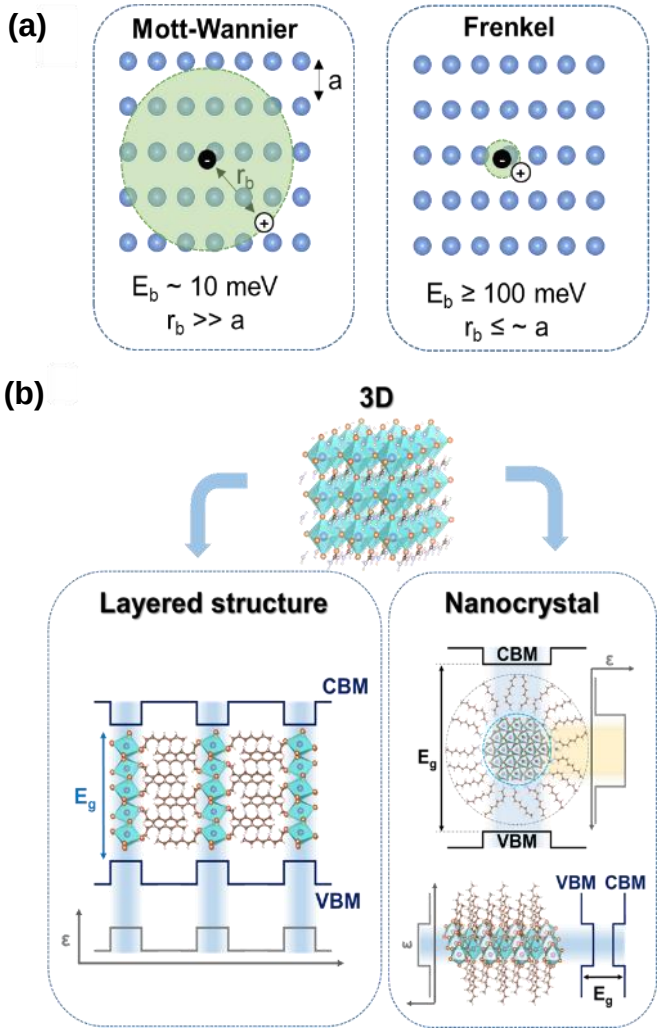

Figure 3: *(a) Illustration of Mott-Wannier and Frenkel exciton and (b) schematic diagram of energy level and dielectric constant scheme of layered perovskites and nanocrystals highlighting the formation of multi-quantum well.*

2.3 Carrier Recombination Dynamics

A good understanding of charge carrier recombination dynamic is of critical importance towards exploiting the exceptional properties of perovskites. Depending on the excitonic binding energy (E_b) of the specific perovskites, photoexcitation can predominantly result in free carriers ($E_b < k_bT_{298K}$) or excitons ($E_b > k_bT_{298K}$). Depending on the number of carriers involved during recombination, photoexcited charge carriers recombine in semiconductors through monomolecular, bimolecular, or Auger recombination processes :[71]

$$\frac{dm(t)}{dt} = G - k_1 m - k_2 m^2 - k_3 m^3 \qquad [1]$$

where *m* stands for the carrier density and *G* is the generation rate. In free carriers system, k_1 is associated with monomolecular recombination constant while k_2 refers to radiative bimolecular recombination coefficient and k_3 points to the Auger recombination coefficient. Monomolecular recombination is associated with trap assisted, whereas bimolecular recombination refers to free carriers recombination processes. Auger recombination involves three carriers where excited electrons non-radiatively recombine with holes to promote another electron to higher energy states (**Figure 4a**). On the other hand, in excitonic system, $-k_3m^3$ component is eliminated from the equation with k_1 refers to radiative germinate / excitonic recombination while k_2 is associated with bi-excitons annihilation (Auger).

Recombination dynamics depend on the carrier density. For example, in the case of 3D perovskites with photogenerated free carriers, at low carrier density, monomolecular trap assisted recombination dominates followed by bimolecular recombination, whereas at very high carrier densities Auger recombination dominates [72]. The radiative efficiency or PL quantum yield (PLQY) gauges the qualities of the materials' optical and electronic properties, with high PLQY indicative of minimal non-radiative recombination losses, which is preferred for optoelectronic applications. High PLQY also supports an efficient photon recycling mechanism that will be beneficial in photovoltaics and photodetectors. PLQY is calculated as:[71].

$$PLQY\ (m) = \frac{radiative\ recombination}{total\ recombination} \qquad [2]$$

Therefore, it is important to minimize the monomolecular trap-assisted and auger recombination rates while maximizing the radiative monomolecular excitonic and bimolecular recombination to attain high PLQY. Hence, the radiative efficiency is also a function of carrier generation (**Figure 4b**). As monomolecular recombination dominates at low carrier generation rates, for 3D perovskites (where free carriers are generated at room temperature) the PLQY is

enhanced with increasing carrier generation due to trap filling effects and reaches a plateau when bimolecular recombination dominates. At higher carrier generation rates, Auger recombination kicks in which reduces the PLQY.

As free charges are generally generated at room temperature due to low E_b, monomolecular recombination is dominated by the trap assisted recombination in 3D $MAPbI_3$ perovskite, which is usually non-radiative [71]. Various techniques such as time-resolved Photoluminescence (TRPL), Transient Absorption Spectroscopy (TA), time-resolved microwave conductivity (TRMC), and time-resolved THz spectroscopy (TRTS), have been utilized to analyze the recombination dynamics. The reported monomolecular recombination rates for $MAPbI_3$ vary between 10^{-7} and 10^{-5} s^{-1} dependent on the film deposition process [73]. On the other hand, the bimolecular recombination ranges between 10^{-9} and 10^{-11} cm^3s^{-1} for both polycrystalline and single crystals[73]. For photovoltaic and light emitting diode applications, the typical carrier concentrations are relatively low (~$10^{15}cm^{-3}$)[71, 74] which aggravate the contribution from monomolecular recombination due to weak bimolecular recombination rates. Therefore, strategies that enhance the excitonic emission, increase local carrier densities or reduce the monomolecular trap assisted recombination to improve radiative efficiency are necessary. Both nanostructures and lower dimensional layered perovskites structures open up new approaches in this regard.

The use of pure layered perovskite itself can increase the E_b that subsequently enhances the excitonic radiative recombination and PLQY [34, 75, 76]. In addition, the carrier cascade effects noted in the mixed dimensional systems that have been of particular interest [13, 74]. Thin films of layered RP perovskites consist of domains with a variety of bandgaps that exist within them. Such a multi-domain structure results in funneling of carriers to the lowest E_g region and subsequent confinement significantly enhances the carrier densities in the emitting perovskite domain. Due to the concentration of the carriers within this emitting domain, bimolecular recombination contribution in the system is enhanced as discussed in detail in section 3.2.

Nanocrystals, on the other hand, confine carriers inside the particles, and concurrently increase both the local carrier density and monomolecular excitonic recombination, boosting radiative efficiency [65, 66]. Thus, PLQY values of up to 95–100% have been reported [47, 48]. Although increasing local carrier density will bypass the slow bimolecular recombination rate, the risk of reducing the Auger recombination onset in the system needs to be taken into account [77, 78]. Although 3D perovskites lag in terms of radiative emission, strategies such as the use

of layered perovskite formations and nanocrystals help to raise the local carrier densities. Additionally, they are effective in confining carriers in the crystal, and passivation of surface defects has been successfully implemented to enhance the radiative efficiency of these materials. In particular, this attribute of maximal radiative efficiency holds significance for applications such as lasers, light emitting diodes, and photovoltaics.

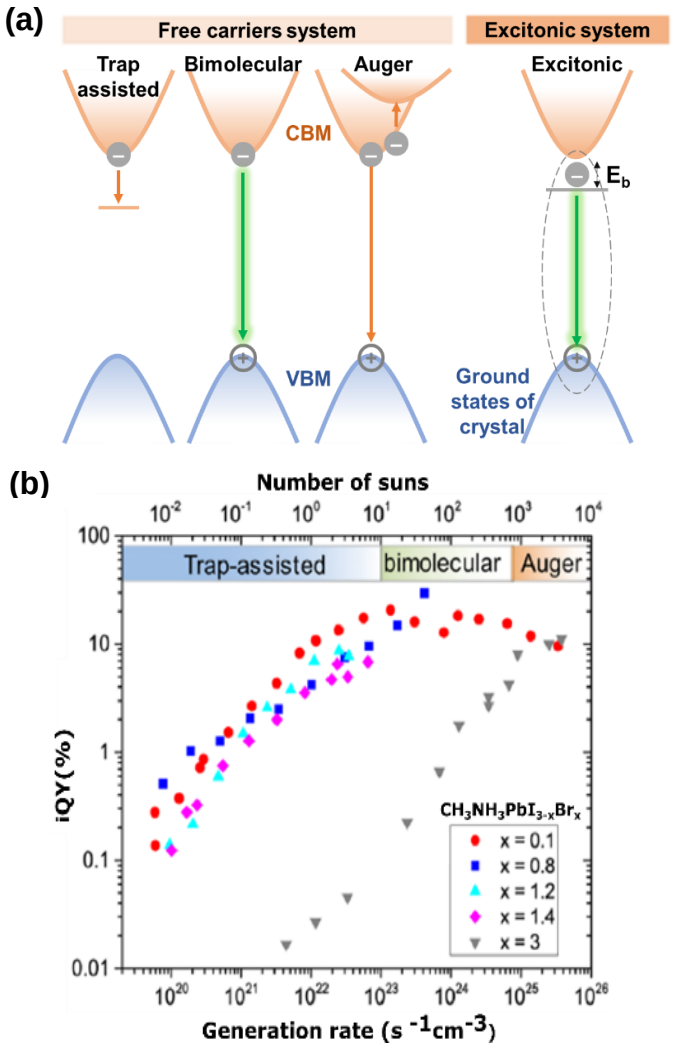

Figure 4. *(a) Schematic illustration of various recombination pathways in semiconductor and (b) Internal quantum yield (also known as PLQY) evolution versus carrier generation for* $MAPbI_{3-x}Br_x$ *films (x varied from 0.1, 0.8, 1.2, 1.4 and 3) reprinted with permission from [72].*

3. Nanostructure and lower dimensional perovskite applications

As described in the previous sections, confined systems such as nanostructures and the mixed layered perovskites have a profound effect on the electronic band structure, carrier dynamics and recombination. These effects brought about by size and structural confinement unlock exciting new properties that may be exploited in optoelectronics and adjacent fields. In this

section we will highlight the main advantages offered by these quantum confined perovskite structures in applications such as solar cells, light emitting diodes, and lasing applications.

3.1 Solar cells

The power conversion efficiency (PCE) of solar cells is defined by the ratio of the electrical energy output from the device to the incident optical power. Although perovskite-based solar cells have shown the remarkable device efficiency improvement within a short time span, susceptibility towards ambient conditions and phase stability are challenges. Films comprised of large grains, high surface coverage with minimum pinholes and fewer grain boundaries offer better charge transport and improved performance [1, 2].These limitations can be overcome by utilizing the perovskite nanostructures and lower dimensional MQW structures [15, 79, 80] . Importantly, we have also highlighted the exotic quantum phenomenon in NCs and in lower dimensional perovskites that can enable approaches that overcome the Shockley–Queisser (SQ) limit such as hot carrier solar cells and multi-exciton generation.

3.1.1. Nanostructured perovskites for slow-hot carrier cooling and multiple exciton generation (MEG)

Theoretical efficiency of a single junction solar cell is estimated to be 33.5%; with transmission, extraction, and thermalization losses making up the rest of the solar energy that cannot be extracted (**Figure 5a**) [81]. Excess kinetic energy of hot carriers ($kT > E_g$) is usually transferred to the lattice via carrier-phonon interactions, commonly known as 'thermalization' or 'carrier cooling' and it is a major limiting factor in photovoltaics. Circumventing the thermalization loss via harvesting hot carriers and MEG would boost the efficiencies beyond the SQ limit, up to 66% and 44% respectively [82-84]. Carrier cooling processes occur rapidly (< 100 fs) [85] in bulk materials due to presence of continuous energy levels **(Figure 5b)** [86], while semiconductor nanostructures with discrete energy levels will reduce carrier-phonon coupling and slow down the carrier cooling (i.e. phonon bottleneck effect - See **figure 5c)** [87].

Slow hot carrier cooling time (~32ps) was noted for the $MAPbBr_3$ NCs (~5 nm – 11 nm diameter) over the bulk film (**Figure 5d)** [23]**.** While other inorganic semiconductor CdSe QDs exhibited rapid hot-carrier cooling with decreasing size, perovskite NCs operating in a weak confinement demonstrated increased cooling times from 10 ps to 32 ps for NCs of size 5 nm and 12 nm respectively [23]. Perovskite NCs have slower hot carrier cooling as compared to CdSe QDs (~0.8ps) or GaAs thin films (~2ps) which is attributed to intrinsic phonon-bottle

neck brought about by a symmetric energy dispersion, small effective charge carrier masses (electrons and holes), and low defect density in perovskite NCs.

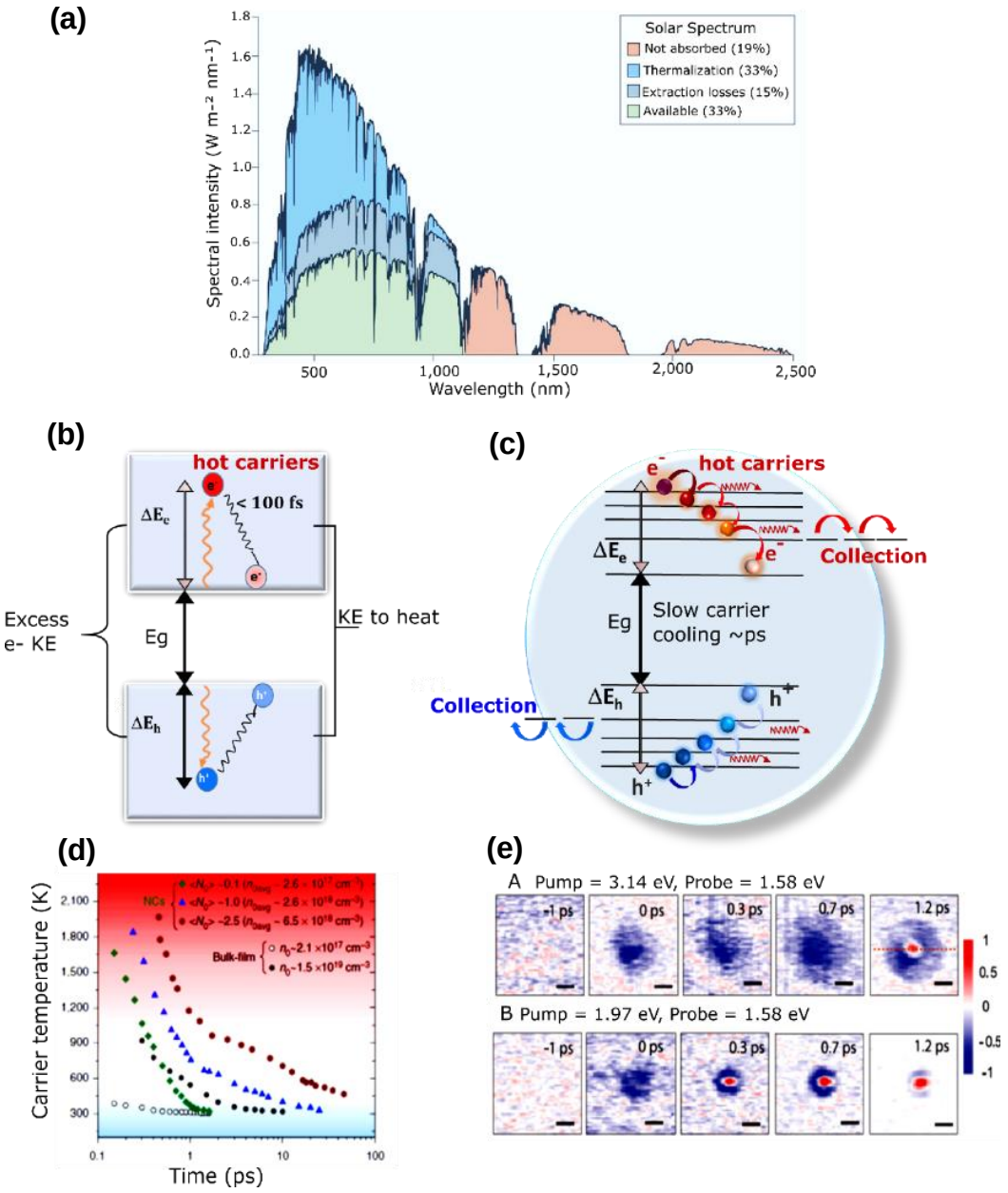

***Figure 5**: (a) Theoretical SQ limit of silicon solar cell with its losses, redrawn from [81].(b) The schematic diagram of hot carrier cooling dynamics in semiconductors bulk films redrawn from [85] and (c) and in Nanostructure, exhibit phonon bottleneck in perovskites NCs redrawn from [87]. (d) Hot-carrier temperature versus delay time for bulk film and $MAPbBr_3$ NCs at various carrier densities reprinted with permission from* [23]. *(e) Ultrafast TAM images recorded at 1.58 eV using 3.14 eV and 1.97 eV pump photon energies at different pump probe delay time indicating transport of hot carrier in $MAPbI_3$ film. Scale bars, 1 μm, reprinted with permission from* [88].

Furthermore, hot carriers extraction by organic layers was also demonstrated with films formed from $MAPbBr_3$ NCs; suggesting that extremely thin absorbers or concentrated solar cells can be the key beneficiaries of the slower hot-carrier cooling from these perovskite NCs [23].

Direct evidence of hot-carrier migration in $CH_3NH_3PbI_3$ thin films was provided using ultrafast transient-absorption microscopy (TAM, **Figure 5e**) [88]. Transport phenomena observed included quasiballistic transport which; was initiated at a pump photon energy of 3.14 eV (1.49 eV above E_g), but was absent at pump photon energy of 1.97 eV (0.32 eV above E_g). Quasiballistic transport (~230 nm) that can overcome grain boundaries and non-equilibrium transport (~600 nm, > 10 ps) before reaching the diffusive transport limit are strong indications of hot-carrier transport. These results suggest potential applications of hot-carrier devices based on perovskites. A substantial population of hot carriers can be retained by slowing down the thermalization processes that occur due to interactions with phonons or the presence of defects. In particular, nanostructures have been shown to be more effective (than bulk materials and thin films) in slower carrier cooling via phonon confinement effects [86, 89].

MEG (conversion of single absorbed photon into two or more excitons) or carrier multiplication (CM) which leads to enrichment in photocurrent. This is yet another means of circumventing the SQ limit in single-junction solar cells. Typically, the MEG process takes place by exciting the semiconductors with incident photon energy greater than E_g (i.e. $h\nu > 2E_g$) **(Figure 6a).** Strongly confined PbSe and PbS QDs were predicted to show enhanced MEG due to relaxed momentum conservation, enhanced Coulomb coupling, and slow hot carrier cooling. However, the phonon bottleneck in these QDs did not materialize due to electron interactions with dense hole states that resulted in faster hot-carrier cooling in smaller QDs. This resulted in the need for higher MEG threshold energies (~$3E_g$), similar to those observed in bulk semiconductors [90, 91].

The potential of MEG in perovskites was highlighted based on the simulated mechanisms of carrier relaxation in $MAPbI_3$ QDs due to quantum confinement effects [92]. Timescales for processes competing with MEG were estimated as: MEG (~fs) < carrier cooling (~ ps) < radiative recombination (ns) < non-radiative recombination (ns) [93]. The main challenge to MEG is linked to both ultra-fast intraband relaxation and Auger recombination, which compete with CM processes[93]. The ideal condition for MEG is to achieve an onset energy twice that of the band gap ($E_{on} > 2E_g$), with negligible non-radiative effects.[92] Highly efficient CM were reported in colloidal $CsPbI_3$ NCs with transient photo-induced bleaching (PIB) dynamics measured below (2.48 eV, **Figure 6b**) and above (4.2 eV, **Figure 6c)** the CM threshold [25].

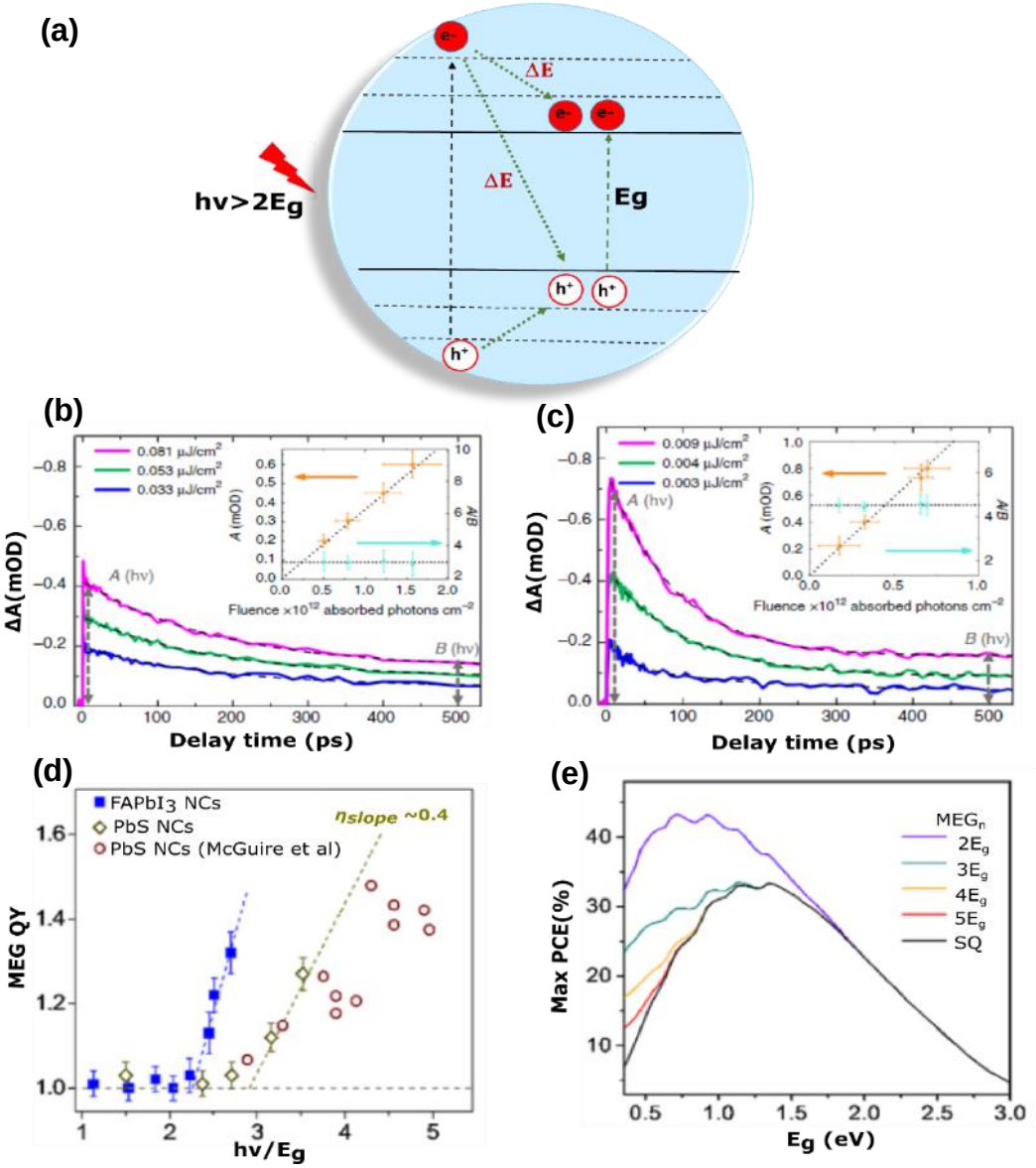

Figure 6: *(a) Schematic representation of MEG process; TA dynamics (b) at pump wavelength of 500nm (2.48eV) i.e below and (c) at pump wavelength of 295 nm (4.2 eV) i.e. above carrier multiplication (CM) threshold for $CsPbI_3$ NCs. Dashed lines denote the exponential data fit. The presence of supplementary fast component at pumping energy 4.2 eV represents CM signature. Inset exhibit single photon absorption (linear) regime, reprinted with permission from [25]. (d) The MEG QY vs hv/E_g of $FAPbI_3$ NCs as compared with PbSe NCs and PbS NCs, reprinted with permission from [94]. The error bars signify the uncertainties in the MEG QY fitting process.* ***(e)*** *Maximum PCEs calculated based on Detailed balance calculations under AM1.5 solar illumination as a function of material E_g for different MEG thresholds. The Shockley-Queisser limit is represented as SQ, reprinted with permission from [24] .*

The presence of the additional decay component, with fast decay time constant for transient PIB above the CM threshold (4.2 eV), is conclusive evidence for CM. Recent studies of colloidal $FAPbI_3$ NCs (7.5 nm), have demonstrated enhanced MEG with threshold photo energy of $2.25E_g$ and slope efficiency up to 75%, which was superior than that reported for strongly confined nanocrystals of PbS or PbSe ($3E_g$) **(Figure 6d)** [24].

Although, PbSe and PbS also benefit from similar small carrier effective masses, the higher MEG thresholds are a result of reduced density of states and increased carrier cooling rates (for smaller QDs), that reverse the advantages of enhanced Coulomb coupling and relaxation of momentum conservation in strongly confined QDs. Low threshold and efficient MEG in $FAPbI_3$ NCs is ascribed to small and similar carrier effective masses and appropriate quantum confinement effect that leads to an inverse Auger process (~90 fs) rendered by the slow cooling of energetic hot carriers. Maximum PCEs based on the detailed balance equation (**Figure 6e,** assuming 100% MEG efficiency under AM1.5) indicates that MEG can help to overcome the SQ limit (~33.5%) and solar conversion efficiencies can reach up to ~44% (**Figure 6e**), with MEG thresholds of $2E_g$ [24, 85]. Thus, the intrinsic phonon-bottle neck observed in perovskite NCs contributes strongly to both slow hot carriers and low threshold MEG observations supporting the potential of beyond SQ limit PVs.

3.1.2. Nanostructured and lower dimensional perovskites for solar cells for improved phase and ambient stability

Efficiency of perovskite-based solar cells has reached up to 25.2%, however susceptibility towards moisture degrade their performance within a short period of time. This is a key challenge in the further development of perovskite-based PV technology and requires highly reproducible and long-term stable high efficiency devices. This limitation is being addressed by implementing layered lower dimensional 2D perovskites in solar cells, which have shown improved stability of the solar cells due to hydrophobicity imparted by the organic molecules [95, 96]. Low formation energy of 3D perovskites leads to their facile decomposition in the presence of moisture. In contrast, intercalation of longer chain organics (e.g. AVA, PEA) between perovskite layers enhances van der Waals interactions, which increases the formation energy of the perovskites and thus minimizes the degradation and improves material stability [97-99]. However, film orientation is an important consideration for charge extraction. This is demonstrated by nanostructures orientated to improve charge transport in mixed-dimensional

($(IEA)_2(MA)_{n-1}Pb_nI_{3n+1}$) perovskite, which yielded efficiency over 9% [100]. Also, device performance of 2D $(BA)_2(MA)_3Pb_4I_{13}$ perovskite was further boosted up to 12.17% by fabricating perpendicularly-oriented films through controlled crystallization processes in a hot casting process (**Figure 7a**) [80, 101].

In 2D perovskites, strategies for overcoming their high exciton binding energies and facilitation of long-lived free carriers are also emerging. Phase-pure homogenous 2D perovskites thin films (for n > 2) revealed exciton dissociation into free carriers, where a fraction of the photogenerated excitons diffuse to the crystal edges and subsequently undergo a conversion to layer-edge states (LESs) [102]. The LES formation minimizes the nonradiative recombination losses and thus excitons can be collected separately as free carriers at their selective contacts [102]. Furthermore, photoinduced electron and hole separation were shown in layered $(BA)_2(MA)_{n-1}Pb_nI_{3n+1}$ perovskite films [103].

This carrier separation is influenced by RP perovskite phases with varying band gaps, which consecutively transfer the photoinduced electron from high band gap phases to small band gap phases, while corresponding hole transport in hundreds of picoseconds [103]. It also highlights the pathways for high efficiency solar cells based on layered perovskites. Even though studies have demonstrated approaches for improved charge transport as well as LES formation to overcome their high E_b limitations, performance of layered perovskites is still challenged by their high E_g which can vary from 1.83 eV for n = 5 to 2.24 eV for n = 1 [104]. Consequently, multidimensional-layered perovskites of 2D/3D bilayer structures have emerged as a promising alternative to overcome the efficiency limit of lower dimensional perovskites, while maintaining the attributes of improved stability [105-107]. In bilayered 2D/3D perovskites, majority of the optical absorption and carrier transport occurs in the 3D perovskite, with the 2D perovskite functioning merely as a hydrophobic capping layer providing moisture barrier, thus enhancing stability. In addition, organic molecules (e.g. PEAI, BAI or OAI etc) integrated on to the top of 3D perovskite layers act as surface passivator, minimizing trap density, reducing non-radiative recombination pathways, and enhancing device performance [108, 109].

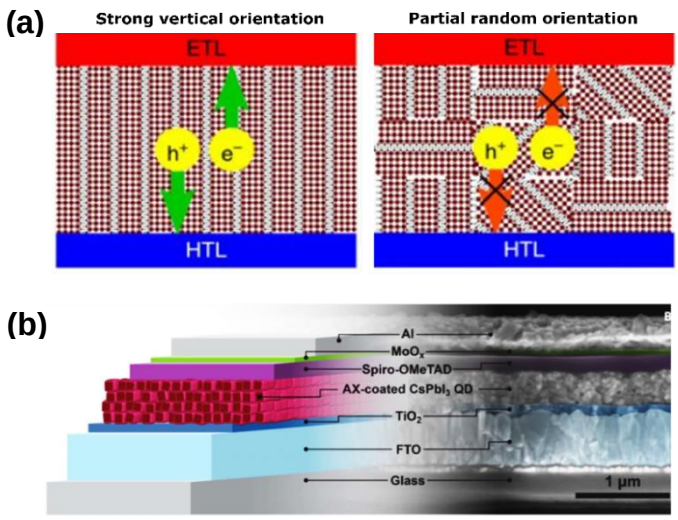

Figure 7: *(a) Schematic representation of vertically orientated lower dimensional perovskites films for better charge collection (left), in comparison with randomly orientation films that hinders effective charge extraction (right) reprinted with permission from[101]. b) The schematic and cross sectional images of high-efficiency FAI-coated $CsPbI_3$ QDSCs device reprinted with permission from [15].*

Thus, the crystallization of 2D perovskite above the 3D perovskite plays a dual role as a hydrophobic barrier as well as surface passivator to improve the device efficiency as well as promote stability. An additional challenge for halide perovskites is their thermal stability, which leads to decomposition at elevated temperature (e.g. $MAPbI_3$ degrades ~ above 85 ^oC) [110]. This issue can be addressed by fabricating an all-inorganic perovskite-based solar cells using Cs cation. However, in thin films, the low bandgap $CsPbI_3$ cubic perovskite phase can be achieved only at high temperature (above 300 ^0C)[111] and degrades rapidly to an orthorhombic β-phase in ambient conditions [112]. However, the high surface energy of $CsPbI_3$ nanocrystals enable stable α-$CsPbI_3$ phase formation at room temperature. Solar cells based on the α-$CsPbI_3$ QDs (~8-15 nm range) have recently been demonstrated with efficiencies of 13.4 % (V_{oc} = 1.2 V) [15] and stability of over 64 days in ambient air. The influence of the insulating ligands on the QD surface was managed by selective ligand exchange and surface passivation. The reported efficiency is also the highest for all-inorganic perovskite solar cells **(Figure 7b)** [15, 79]. Solar cells fabricated with $MAPbI_3$ NWs exhibited device performance of 14.7%, which is attributed to excellent photo carrier extraction due to lateral conductivity of 5.86 x 10^{-10} S/m; which is 1.6 times better than those in 3D cubic crystal structures [113]. Although NW and QD approaches are likely to offer better stoichiometric control and offer effective phase stabilization, challenges with these nanostructures include exciton formation, reduced diffusion lengths, anisotropy in charge transport, and increased surface recombination, amongst others.

Thus, countering the effects of increased recombination due to smaller grains and reduced charge carrier diffusion lengths are essential if high efficiency solar cells are to be realized with these nanostructures.

In addition, although the bandgap of the perovskites can easily be altered by employing mixed anions, photo or current induced halide segregation limit their performance and stability during device applications [114]. Lower dimensional or nanocrystal perovskite formation proved to be advantageous in tackling the phase segregation problem in mixed halide perovskites [22, 114, 115]. For instance, $CsPb(I_{0.5}Br_{0.5})_3$ perovskite nanocrystals demonstrates spectrally stable PL under photo excitation as opposed to the bulk counterpart due to the smaller carrier diffusion length and injected carrier densities [116].

3.2 Perovskites for efficient LEDs

Quantum confinement and related properties of the perovskite nanostructures also open up further opportunities especially in the fields of light-emitting diodes (LEDs) and lasing. Perovskite LEDs (PeLEDs) with EQE evolution from below 1% to exceeding 20% have been reported within 5 years [117-119]. This marvellous progress is due in part to their tunable intrinsic properties (e.g. E_g, E_b), defect tolerant nature, and technology transfer from the mature perovskite-based photovoltaics fields [20, 21].

The external quantum efficiency (EQE) of LED measures the number of photons emitted with respect to the number of electrons flowing through the devices. Carrier confinement with high E_b materials are preferred to construct efficient electroluminescence (EL) devices. High EL efficiency can only be accomplished by circumventing non-radiative recombination, which typically occurs through defect or trap states (trap-mediated recombination). In typical PeLED operating conditions, charge-carrier densities of $\sim 10^{15}$ cm^{-3} are observed, comparable to trap densities reported in 3D perovskites [120, 121]. Thus, the EQE in perovskite films is determined by competing processes of trapping at defect-states (first order decay process) versus slow electron-hole bimolecular radiative recombination (second order decay process) and their lower E_b (~9-50 meV) [122]. Under thermodynamic equilibrium conditions, depending on E_b and the excitation energy, coexistence (and interactions) of free charges and excitons is likely to affect radiative recombination. Therefore, one method to achieve high-efficiency PeLEDs has been through controlling the NCs size and by employing lower-dimensionality perovskite emitters that would spatially confine carriers leading to enhanced radiative recombination [123]. Efforts to enhance PLQY and EQE of PeLEDs by utilizing

layered lower dimensional system and physically confined carriers in nanograins or NCs will be reviewed in depth below and summarized in table 1.

3.2.1 PeLEDs based on small grain size thin films and lower dimensional systems

In 1994, initial efforts on LED based on 2D lead based perovskite compounds can achieved EL at liquid nitrogen temperatures [124] and at very high applied voltage[125]. Recently, room temperature EL was demonstrated by employing 3D perovskites films, however PeLED performance (EQE) was restricted below 1 % due to large grain size and poor surface coverage film formation, which resulted in high nonradiative recombination, and lower PLQY [4, 20, 120, 123, 126]. Strategies to enhance the PLQY are crucial to boost the EQE and as a follow up the formation of small grain size are preferred to spatially limit carrier diffusion thus enhancing the radiative recombination [65, 127-130]. PeLEDs fabricated by utilizing a small grain $MAPbBr_3$ emissive layer have managed to achieve a current efficiency (CE) of 42.9 cd A^{-1} with an EQE of 8.53% (**Figure 8a and 8b**). The improved performance is attributed to carrier confinement within the small grain size as well as reduced nonradiative recombination centres induced by Pb metallic phase [127]. Further, the approach of controlling perovskite grain size by means of the addition of long chain organic cations or polymers led to the perovskite films with nanocrystal like morphology with enhanced PLQY as well as device performance [131-133].

Furthermore, all inorganic perovskite $CsPbBr_3$ films fabricated using cesium trifluoroacetate (TFA) demonstrated efficient (CE of 32.0 cd A^{-1} and EQE of 10.5%) and stable green LEDs with a half-lifetime over 250 h at 100 cdm^{-2}. The improvement in efficiency and stability is attributed to improved crystallization and overall molecular structure of $CsPbBr_3$ films. The addition of TFA in the perovskite precursor enhances the interaction of TFA^-anions (CF_3COO-) with Pb^{2+} cations improving the crystallization, while the strong electronegativity of F enhances the structural stability of $CsPbBr_3$ perovskites [134].

Utilizing quasi 2D perovskites which can also boost the PLQY due to energy landscape formation that promotes carrier cascade to lower bandgap (3D domain) enhances the radiative recombination and hence device performance (EQE) [11, 13]. In response, device EQE can be boosted up to 12.2% by harvesting carrier funnelling effect on the quasi 2D perovskites [135]. Furthermore, surface traps and grain boundary defects have hindered the performance of LEDs, successively surface passivation with trioctylphosphine oxide (TOPO) has provided another

avenue to boost the PLQY, resulting in devices with CE of 62.4 cd A^{-1} and EQE of 14.36% [135].

A mixed halide approach (Br/Cl) to obtain blue PeLEDs (450 – 490 nm) has been impeded due to halide ion migration which triggers phase segregation issue under applied bias [136-139]. However, this limitation can be overcome by fabricating mono halide quasi-2D perovskites film with combination of long chain PEA and shorter chain cation (e.g. iso-propylammonium, IPA), which resulted in controlled crystallization of perovskites to higher 'n' quasi 2D domain, with maximum luminance of 2480 cd m^{-2} (λ = 490 nm) [140]. Overall, perovskite grain size, balanced charge injection, and surface and grain boundary passivation are the critical parameters we need to pay further attention to in order to boost the performance as well as stability of PeLEDs.

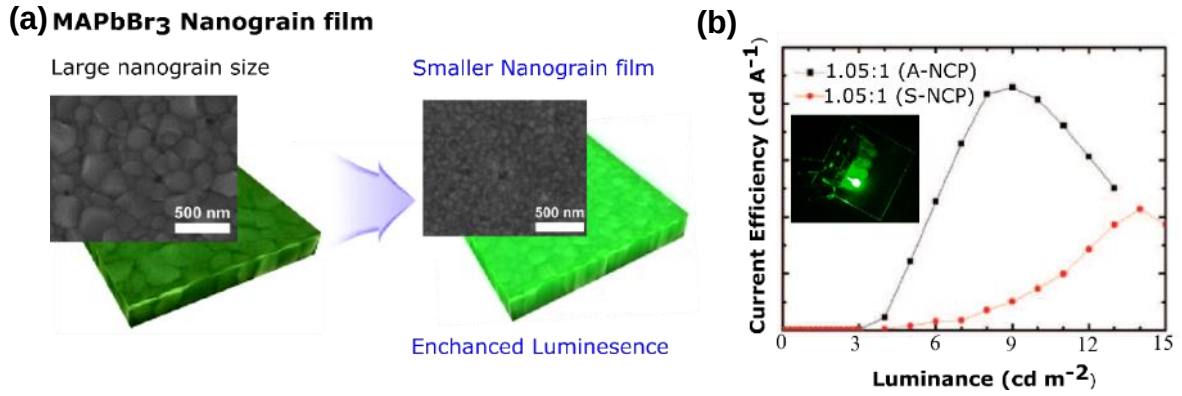

Figure 8: *(a) SEM image and corresponding optical image of $MAPbBr_3$ perovskite films with larger nanograin size and smaller grain size and (b) and corresponding PeLED characteristic: current efficiency vs luminance. The films were prepared with MABr:PbBr (1.05:1) precursor composition with solvent-based nanoscrystal pinning (S-NCP) technique for larger nanograin size and additive-based NCP (A-NCP) technique for smaller nanograin size, insert shows photograph of PeLED device reprinted with permission from[127].*

3.2.2 PeLEDs based on perovskite colloidal NCs

The high PLQY of NPs is mainly attributed to their high E_b because of effective exciton confinement in small size particles (< 20 nm) as compared to polycrystalline (grain sizes > 100 nm) perovskite films. Initial reports of NC, NPL, QD PeLEDs [141] even with high PLQY (≥ 85 %) were demonstrated relatively low EQEs (< 1 %) [29]. This was attributed to the insulating nature of the emitter layer due to surface capping ligands. Controlled synthesis,

purification and post synthesis treatments were effective in controlling the amount of surface ligands [29, 142-144] to achieve better performance [29, 145-147]. Interestingly, energy or charge cascade mechanism was observed in formamidinium lead bromide ($FAPbBr_3$) NCs which in return exhibited PLQY over 80% and CE of 57.6 cd A^{-1} with an EQE above 13% at 530 nm (***Figure 9a and 9b***). Additionally, power efficiencies of more than 58 lumens per watt without light-out coupling structures were also reported [26].

Furthermore, the challenge to obtain red emissive PeLEDs (625 – 740 nm) can also be overcome by employing $CsPbI_3$ derivatives. The instability of the PL-active α phase (cubic) $CsPbI_3$ [79] can be resolved by utilizing the high surface energy of nanocrystals which stabilized the α phase at room temperature [47]. Due to the weak acid –base interactions between the I- (weak base) and the oleylammonium ligand (a hard acid) as compared to Br- (strong base), isolation of $CsPbI_3$ QDs is more challenging while the loss of ligand during QDs purification causes agglomeration and hence conversion to the PL – inactive orthorhombic phase [79]. Antisolvent that selectively removes excess ligand only, such as methyl acetate, can be employed to prolong the α phase stability for months [79]. QDs synthesized with the mixed cation or anion approach is also one of the best approaches reported for phase stabilization [79, 136, 148]. For example, synthesizing FA-doped $CsPbI_3$ NCs (10−15 nm), isostructural to the orthorhombic $CsPbBr_3$, exhibited PLQY > 70% and EQE 2.3%. Employing anion exchange method to convert stable cubic $CsPbBr_3$ to cubic $CsPbI_3$ at room temperature demonstrated an EQE of 21.3% at 649 nm [119]. Controlled chemical composition and optimum amount of surface ligands are critical parameters for high EQE and stability of PeLEDs based on anion-exchanged perovskite QDs **(Figure 9c).**

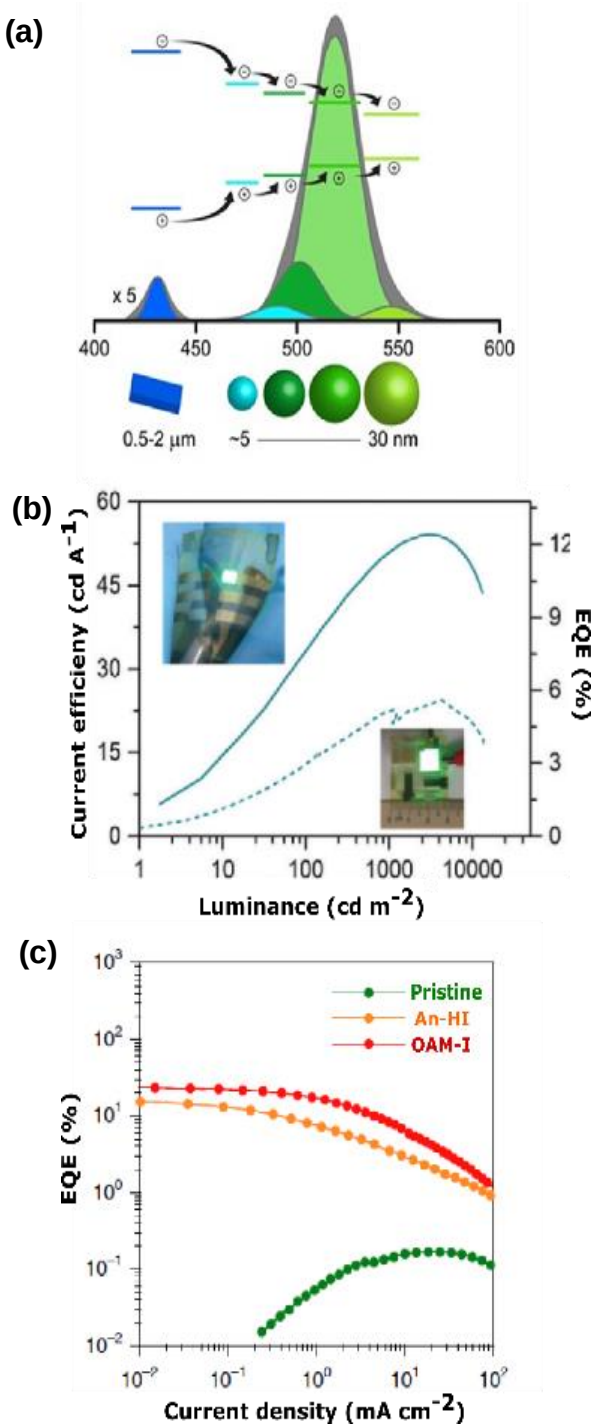

***Figure 9**: (a) Schematic representation of charge carrier transfer process from 2D microplates to NCs of graded size, and from smallest size (larger band gap) to largest size (smallest bandgap) NCs of mixed FA and octylammonium lead bromide system. Deconvolution of steady-state PL illustrates the PL contribution from different size domains; (b) Current efficiency and EQE at different luminance for 3 mm^2 flexible and 95.2 mm^2 large area $FAPbBr_3$ NCs based PeLED devices, reprinted with permission from* [26]. *(c) Current density–voltage–luminance curves of perovskite QD LEDs of pristine $CsPbBr_3$, OAM-I treated and An-HI treated QDs with insert showing TEM images of An-HI treated QDs (scale bar 20nm), reprinted with permission from [149].*

Table 1: Summary of the recent advances in blue, green, and red PeLEDs fabricated using lower dimensional and perovskite nanostructures as an emitter layer. The organic capping ligands used in the preparation of nanostructures are also indicated. EL – electroluminescence, V_{th} –turn on voltage, L_{max}-maximum luminance, EQE –external quantum efficiency.
Abbreviations: Ethylamonium bromide : EABr, Butylammoniumiodide / bromide : BAI / BABr, Phenethylammonium iodide / bromide : PEAI / PEABr, naphthylmethylamine iodide : 1-NMAI, 4-phenylbutylamonium iodide / bromide : 4-PBAI / 4-PBABr, Octylammonium bromide : OABr, 2-phenoxyethylamonnium bromide : 2-POEABr, isopropylammonium bromide – IPABr.

Perovskite Emitter	EL (nm)	V_{th} (V)	L_{max} ($Cd.m^{-2}$)	EQE (%)	Ref
Lower dimensional perovskites					
BAI : $MAPbI_3$	750			10.4	[150]
BABr : $MAPbBr_3$	520			9.3	
PEAI : $MAPbI_3$		3.8		8.8	[13]
1-NMAI :$FAPbBr_xI_{3-x}$	763	1.3		11.7	[151]
1-NMAI : $CsPbI_3$	694	1.9	732	7.3	[152]
4-PBAI : $CsPbI_3$	683			7.3	[153]
4-PBABr : $CsPbBr_3$	514	2.8	14000	10.4	
Cs_2PbI_5	693	4	120	0.14	[154]
Cs_2PbBr_5	520	3.8	7317	1.1	
PEABr : $MAPbBr_3$	526		8400	7.4	[155]
PEA : $CsPbBr_3$	514	3	11536	3	[132]
OABr: $FAPbBr_3$	540, 505	2.2		5	[11]
PEABr : $FAPbBr_3$	532	3	9120	14.36	[135]
POEABr : $MAPbBr_3$	506, 520 480, 494, 508 462	~3.3 ~3.5 ~6.2	64.2 19.25 1.26	2.82 1.1 0.06	[156]
EABr: $MAPbBr_3$	473	2.4	200	3	[99]
PEA_2PbBr_4	410	2.5		0.04	[157]
PEABr : IPABr: $CsBr_xMA_{1-x}PbBr_3$	490	~5.4	2480	1.5	[140]
BABr : $CsPbBr_xCl_{1-x}$	487	4.5	3340	6.2	[158]
BABr : $CH_3NH_3PbBr_3$	~440, 460, 475	~5	1	5.4 x 10^{-3}	[138]
PEABr : $CsPbBr_xCl_{3-x}$	480	3.2	3780	5.7	[159]
Perovskite Nanocrystals					
$CsPbI_3$ NC_S (Oleyamine : oleic acid)	698	NA	206	5.7	[160]
$CsPbBr_3$ NCs (Oleyamine : oleic acid, aniline hydoroiodide / oleylammonium iodide)	645	2.7	NA	14.1	[119]
	653	2.8		21.3	
$CsPbBr_xI_{3-x}$ NCs (Oleyamine : oleic acid)	648	1.9	2216	6.3	[161]
$CsPbBr_3$ NCs (Oleyamine : oleic acid : Cesium stearate)	527	4.6	3853	2.21	[162]
$FAPbBr_3$ (Oleic acid : octylamine)	530	2.2	34480	13.4	[26]

$FAPbBr_3$ (Oleic acid : octylamine)	530	~3	~700	2.05	[16]
$Cs_xFA_{1-x}PbBr_3$ (Octylamine : oleic acid)	525	3.5	55005	2.8	[139]
$CH_3NH_3PbBr_3$ (Octylamine)	513	2.8	11830	3.8	[163]
$Cs_xMA_{1-x}PbBr_3$ (Oleylamine : oleic acid)	523	3	24510	1.3	[164]
$CsPbBr_3$ (Oleyamine : oleic acid)	512	2.6	1660	8.73	[165]
$CsPbBr_3$ (Oleyamine : oleic acid)	512	3.4	15185	6.27	[147]
$CsPbBr_xCl_{3-x}$ (Oleyamine : oleic acid)	516 452	4.2 5.1	946 742	0.12 0.07	[141]
$MAPbBr_3$ (Oleic acid : octylamine)	456	~5.6	2	2.4 x 10^{-3}	[166]
$CsPb_yMn_{1-y}Br_xCl_{3-x}$ (Oleyamine : oleic acid :$MnCl_2$)	466	~4.2	245	2.12	[167]
$CH_3NH_3PbBr_xCl_{3-x}$ (Octylamine : oleic acid)	445	~7.8	2673	1.38	[168]
$CsPbBr_xCl_{3-x}$ NCs (Oleyamine : oleic)	490	3	35	1.9	[169]

3.3 Perovskite-based nano lasers

Semiconductor lasers are miniaturized amplified coherent light sources that have potential applications in various fields such as optical communication, computing, and imaging, etc [170-173]. Light amplification per unit length is defined as optical gain while the input energy at which transition from spontaneous emission (SE) to amplified SE (ASE) occurs is referred to as the ASE threshold. Semiconductor materials like CdSe QDs, CdSe/CdS QDs, GaAs NWs, and InGaN/GaN MQW have been demonstrated for lasing (ASE), however, their high threshold carrier densities and non-facile fabrication (material lattice mismatch and incompatible growth temperature) obstruct their application and integration into optoelectronic devices. The high absorption coefficient and defect tolerant nature of perovskites promise excellent optical gain materials for lasing application. In 2014, the transition from SE to amplified ASE with increasing pump fluence has been demonstrated in solution processed $MAPbI_3$ film with ASE thresholds as low as 10 ± 2 μJcm^{-2} (***Figure 10a***) [6]. In another work, $MAPbI_3$ perovskite film (~ 70nm, grain size ~140nm) prepared using atomic layer deposition (ALD) method, reported gain of 3200 cm^{-1}. The possible reasons for high gain value could be a small grain size, controlled thickness (in nm), uniform and defect free film formation [174].

Critical criteria for achieving improvements in ASE includes suppression of bulk defect density (e.g. vacancies, interstitials, antisites) and reduction of the multi-particle non-radiative

recombination in the gain media. In addition, longer carrier lifetimes (~ns), high PLQY, wavelength tunability over visible range as well as capability to attain population inversion are all essential parameters for ideal lasing materials [57, 175, 176]. Perovskite NCs as well as low dimensional systems have been explored as a gain medium to achieve better performance at a low cost fabrication method [136, 148, 177]. Due to differences in refractive index between perovskite and the environment, natural formation of Fabry-Perrot cavities and whispering gallery mode cavities can be found in NWs [173, 178] and NCs [179] which potentially could eliminate the need to deposit additional passive optical cavities to produce laser devices.

For example, 10 nm sized $CsPbX_3$ NCs (X = Cl^-, Br^-, or I^-) demonstrated low ASE - thresholds (5 ± 1 μJ cm^{-2}) with a net gain of 450 ± 30 cm^{-1} over the entire visible spectral range with natural whispering gallery mode cavity (***Figure 10b and 10c***) [179]. The obtained optical gain values were superior to other chalcogenide nanostructures (e.g. CdSe, CdSe/CdS) [180, 181], and were attributed to the absorption cross-section (σ) of $CsPbBr_3$ perovskite NCs (8×10^{14} cm^2) that was two orders of magnitude larger than CdSe QDs[182]. Low ASE thresholds had also been reported $FAPbX_3$ (X= Br^- and I^-) NCs [183, 184], $MAPbBr_3$ NCs[185-187], and $CsPbX_3$ (X = Cl, Br, I) NWs, NPLs [188] as well as lead free $CsSnI_3$[189] and $FASnI_3$ [190] thin films. Moreover, an ultralow lasing threshold (0.39 μJ/cm^2) with notably superior device stability (5 h/ 1.8×10^7 optical pulse excitations) under ambient conditions had been demonstrated when $CsPbBr_3$ QD were incorporated between two highly reflective distributed Bragg reflectors (DBRs) as passive optical cavities [191].

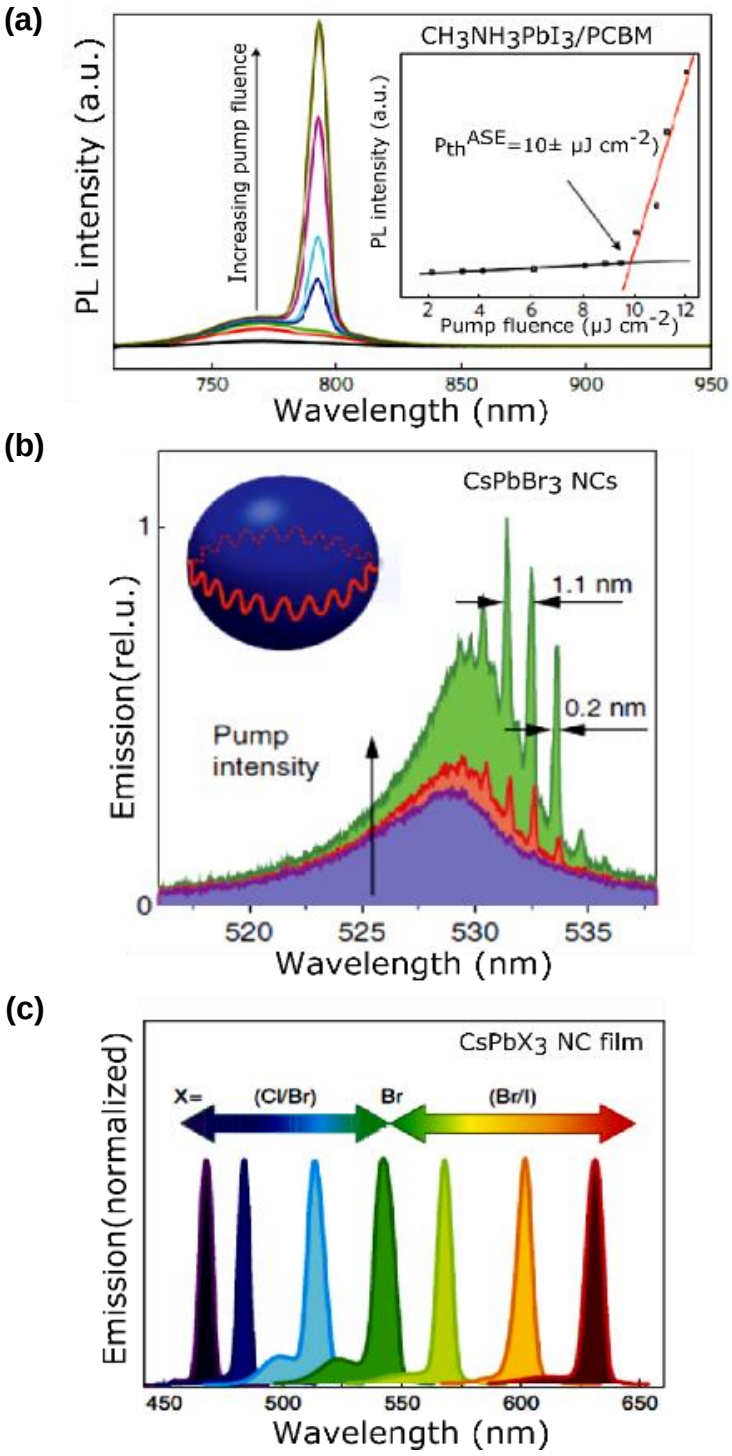

Figure 10: *(a) The pump fluence-dependent PL spectra of $CH_3NH_3MAPbI_3$(65 nm)/PCBM films. The PL intensity vs pump fluence in the inset with black and red lines denote the linear fits to experimental data in SE and ASE linear region respectively, reprinted with permission from [6]. (b) PL evolution with respect to pump intensity in a microsphere resonator (15 mm) covered by $CsPbBr_3$ NCs film and (c) Spectral tunability of ASE with compositional variation of $CsPbX_3$ NCs thin films, reprinted with permission from [179].*

Perovskite-based NW lasers are promising building blocks for fully integrated nanoscale photonic and optoelectronic devices. Each NW can act as a waveguide along the axial direction and its two end facets form a Fabry-Perot cavity for optical amplification [173, 178]. Wavelength-tunable lasing, at room temperature, from single-crystal $MAPbX_3$ perovskite NWs with very low lasing thresholds (220 nJ cm^{-2}) at low charge carrier density (1.5 x 10^{16} cm^{-3}) and high quality factor (Q~3,600) have been demonstrated [30]. This quality factor (Q ~3,600) is more than an order of magnitude higher than that from the state-of-the-art GaAs-AlGaAs core-shell NW laser operating at a temperature of 4 K [192]. Interestingly, the emission image of the NW exhibits uniform intensity from the whole NW below ASE threshold and shows strong emission with spatial interference from the two coherent light sources at the two end facets above the ASE threshold and shows strong emission with spatial interference from the two coherent light sources at the two end facets above the ASE threshold. This is mainly due to the difference in the refractive index between the nanowire and its environment (atmosphere, substrate, etc.), which generates significant end facet reflectivity as well as efficient wave guiding along the length of the wire and axial Fabry-Perot cavity modes. These are favorable conditions to create a NW as a single-mode waveguide and laser resonator, which is capable of lasing with relatively low excitation thresholds. Nevertheless, the mechanism for optical gain by stimulated emission in perovskite nanostructures is still under investigation. The lasing threshold depends on dimensions, end facets and crystalline quality of the NWs [193, 194]. For the NWs of smaller length (7.5 μm) mainly one lasing peak has been observed, and for longer NWs (13.6 μm and 23.6μm), multiple and equally spaced lasing peaks are observed which corresponds to the waveguide mode origin. The 'top-down' approach for large-scale $MAPbX_3$ perovskite nanowire arrays fabrication using the polydimethylsiloxane rectangular groove template (RGT) enhances the photostability with an operation duration exceeding 4×10^7 laser pulses. The method is highly compatible with lithographic techniques and are important for integrating NW in optoelectronic devices [193].

$CsPbX_3$ NWs reported an onset of 5 μJ cm^{-2} with a quality factor of 1,009 ± 5 (***Figure 11a and 11b)***. In addition, high device stability under near-ambient conditions as well as under constant lasing, pulsed excitation for over 1 h (equivalent of 10^9 excitation cycles) have been demonstrated [194]. $CsPbX_3$ NWs prepared using the chemical vapor transport method exhibit a uniform growth direction, smooth surfaces, straight end facets, homogeneous composition distributions, low lasing threshold (3 μJ/cm^2) and high Q factors (1200-1400) under ambient atmospheric environments [195]. Recently approaches to scalable ambient NWs preparation

were reported, opening possibilities for fully integrated nanophotonic and optoelectronic applications. For example, $CsPbBr_3$ NWs (4.3 μm) inks prepared by water mediated ligand assisted reprecipitation have been reported which can be deposited via scalable spray casting method at ambient conditions for lasing application (lasing thresholds 13 μJ cm^{-2} with Q = 1017) [196]. In another approach, scalable $CsPbBr_3$ nanowires were deposited via a short distance gas phase deposition technique (triggered by temperature differences between growth substrates and solution processed $CsPbBr_3$ thin films source) by using a simple hot plate. The lasing characteristics were reported at thresholds of 27.3 μJ cm^{-2} and Q factor of 1330 [197].

In recent studies, energy cascading effect on RP perovskites ($BA_2FA_{n-1}Pb_nBr_{3n+1}$) have also been shown to boost the optical gain as well as dramatically reduce the ASE threshold as compared to 3D counterparts. Nanolasers based on RP perovskites NWs were made using a PDMS template to confine the growth and room temperature ASE was reported with quality (Q) factor (ca. 1800) and low lasing thresholds (27 - 31 μJ cm^{-2}) [198]. The refractive index differences between lower dimensional and higher dimensional perovskites in mixed RP system ($OA_2MA_{n-1}Pb_nBr_{3n+1}$) microplatelets also served to confine both exciton and photon resulting in higher optical gain and reduced ASE threshold [14]. Thus nanostructured hybrid perovskites (e.g. NCs, NWs and NPLs) can themselves act as optical modulators and are favorable to achieve low lasing thresholds and high-quality factors. Furthermore, high-performance lasers can also be fabricated by integrating the dielectric nanostructured gain medium in a photonic crystal cavity [199, 200].

Other confinements and resonant phenomena have been also noted in perovskite nanostructures. When the dimension of a spherical nanoparticle is comparable to the photon wavelength (200 – 1000 nm), each nanosphere would generate geometric Mie resonant. At low order mode, PL at the Mie resonances will be enhanced [201], while a higher order Mie resonant mode can support ASE. This has been shown in single mode laser detected from 0.2 – 10 μm $CsPbX_3$ (X = Cl, Br, I) microsphere at thresholds as low as 0.42 μJ cm^{-2} [202]. Fano resonances, which originate from interaction between exciton and Mie resonances, have been observed in isolated perovskite nanoparticles which would be beneficial for on chip integrated light emitting nano antenna [201, 203].

Furthermore, periodic resonant perovskite nanostructures can create either photonic crystals (i.e. when the period of the array is large enough to diffract photon) or metasurfaces (i.e. when the period is smaller than the size required to diffract photon). In either case, the light localization can be enhanced specifically at certain wavelength depending on the structure

which potentially can be used to tailor the optical properties of the material [199, 200, 204, 205] For example, perovskites with metasurface structure with nanoslit embedded in perovskite thin films can be used to tune the colour of the perovskites as well as enhance the PL intensity of the materials due to Purcell effect [206].

Strong coupling between excitons and cavity confined photons is called exciton polaritons. Various cavities and resonances can be used to enhance the interaction rate between exciton and cavity confined photons, such as Bragg reflector cavities [207], surface plasmonic cavities [208] etc. Polariton lasing is promising for ultralow threshold lasing as population inversion is no longer needed. It has been observed for CdTe and GaAs, InP at cryogenic temperatures [209-211]. Materials such as ZnO and GaN have displayed room temperature polariton lasing. However, epitaxial techniques were deemed essential to ensure high quality microcavity and gain medium fabrication [212, 213]. Although the Frenkel exciton nature of organic media possesses attributes of large exciton binding energy and ease of fabrication, the weak coulomb interactions lead to inefficient polariton relaxation which results in higher threshold density and weaker nonlinearity as compared with inorganic gain media [214]. Nanostructured perovskites offer large exciton binding energy, ease of fabrication, and excellent optical properties; and room temperature, polariton lasing in $CsPbCl_3$ nanoplatelets planar microcavity has been demonstrated with ASE threshold as low as 12 μJ cm^{-2} despite the use of low Q cavity (~300) [215]. Halide perovskites have also been investigated for two-photon-pumped laser development with encouraging reports of strong two-photon absorption (TPA) and ease of achieving population inversion [216, 217]. TPA enables longer excitation penetration depths, which can effectively be utilized for three-dimensional material microfabrication,[218] bioimaging [219] and data transmission [220, 221]. Two-photon pumped microlasers from perovskite microwires [222] and band-to-band photoluminescence have also been demonstrated for $MAPbBr_3$ single crystals [223]. Perovskites have also been demonstrated to possess large multiphoton absorption (MPA) 'action cross-sections' (σ x η; σ: MPA cross-section, η: PLQY) for core-shell $MAPbBr_3/(OA)_2PbBr_4$) NCs (***Figure 12a to 12c***) [27].

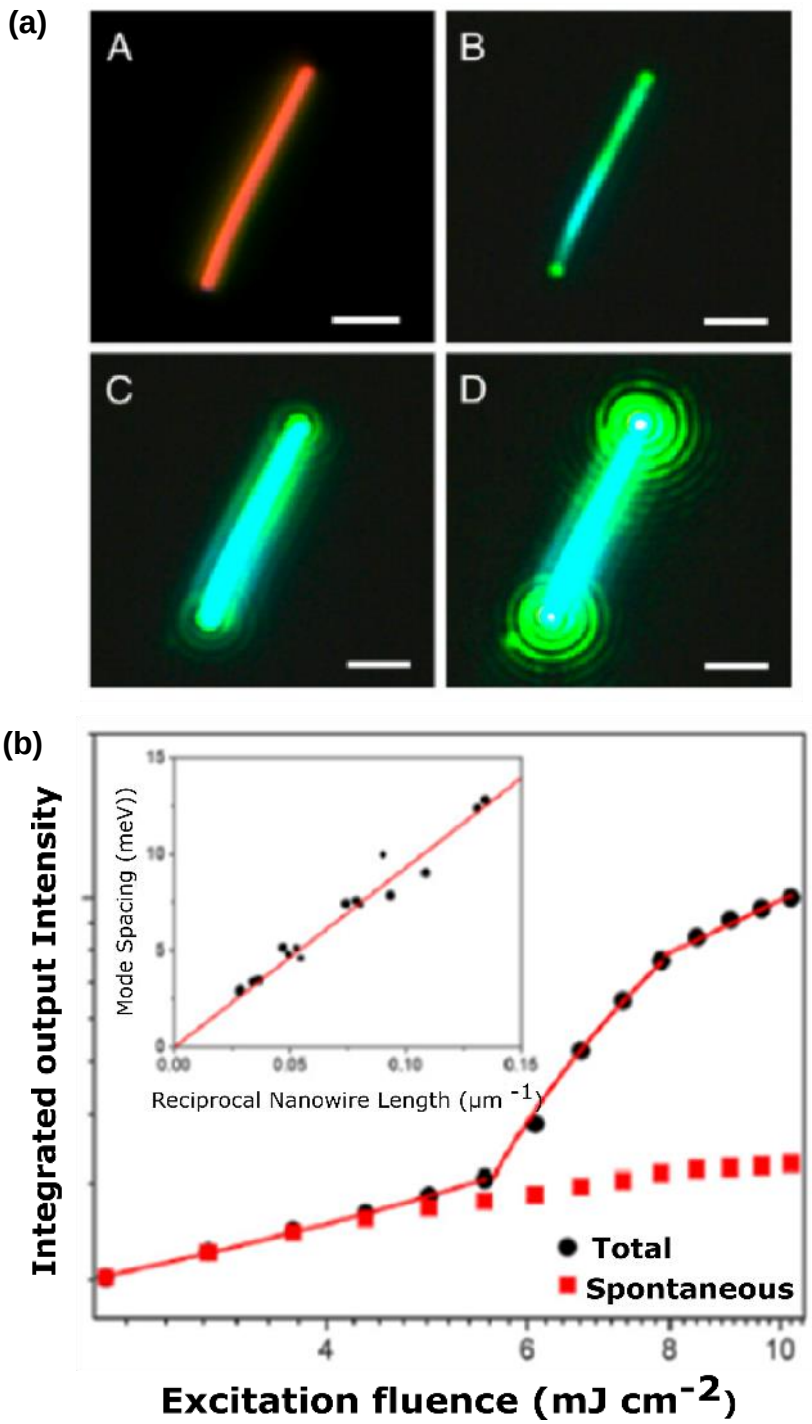

Figure 11: *(a) The dark field single-crystal $CsPbBr_3$ nanowires (A) and lasing images with increasing excitation fluence (B-D) (scale bar: 2 μm); (b) followed by the integrated output intensity vs pump fluence of the $CsPbBr_3$ nanowire (black circles) with typical S-curve indicating three emission regime: spontaneous emission (<5 μJ cm^{-2}), amplified spontaneous emission (5–10 μJ cm^{-2}), and lasing (>10 μJ cm^{-2}). The mode spacing vs reciprocal nanowire length graph confirms the Fabry Perot lasing (inset). All figures are reprinted with permission from [194].*

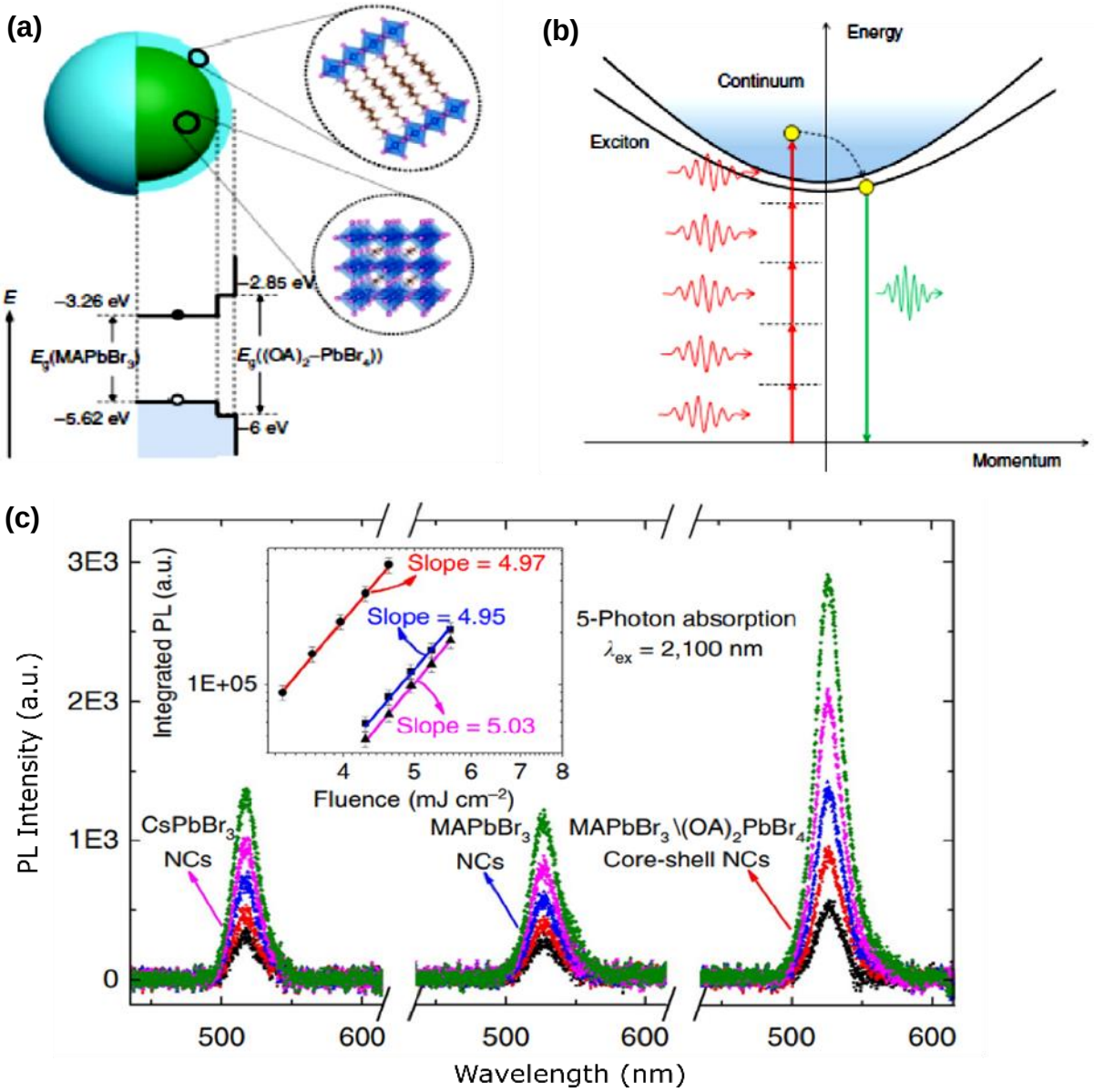

Figure 12: *(a) Illustration of core–shell multidimensional perovskite NCs with 3D $MAPbBr_3$ as core and 2D $(OA)_2PbBr_4$ as shell with their type-I energy level alignment followed by the (b) illustration of five photon absorption process in NCs. (c) The photoluminescence spectra from core-only $MAPbBr_3$ NCs, core–shell $MAPbBr_3/(OA)_2PbBr_4$ NCs and $CsPbBr_3$ NCs at 2100 nm excitation are presented with signature of five photon absorption phenomena. Figure c inset reveals the quintic dependence of integrated PL intensity on the excitation fluence. Figures a-c are reprinted with permission from* [27].

The MPA cross-sections of core-shell NC were 3 to 10 times superior compared with similar NCs made from $MAPbBr_3$ and $CsPbBr_3$. This enhancement in the MPA action cross section is

attributed to strong confinement regime, with $(OA)_2PbBr_4$ shell formation over the $MAPbBr_3$ core [27]. The MPA effects in perovskite core-shell NCs were also 1–2 orders larger than that of CdSe/CdS nanostructures, ZnSe/ZnS core-shell NCs. Furthermore, the five-photon action cross-sections for core shell NCs [27] were almost nine orders larger than the best reported organic molecules.

4. Summary and Outlook

Perovskites have delivered astounding results in photovoltaics, light emitting devices, and lasers. However, the quantum confinement effects and the promise that they offer to challenge the optoelectronic limits are just beginning to be considered.

Confinement, that can be readily achieved in the MQW structures in layered perovskites or through nanostructuring, has a profound impact on electronic band structure, carrier dynamics, and recombination dynamics. Layered perovskites shrink bandwidth of CBM and VBM, form Frenkel excitons, increasing both E_g and E_b, thus enhancing radiative recombination. Nanostructuring with NWs, NPLs, and NCs form discrete electronic structures, concentrating carriers inside the nanostructures increasing both the local carrier density and monomolecular excitonic recombination. The possibility of modulating the photoexcited state by modulating the choice of organic spacers; and symmetric energy dispersion, relaxed momentum conservation, and enhanced Coulomb coupling brought about by size modulation provides further credence to the exceptional properties and versatility offered by metal halide perovskite semiconductors. Surface ligands play a very important role by providing passivation of surface defects as well as effectively confining the charge carriers.

The exotic quantum phenomena in NCs can enable approaches that overcome the SQ limit such as hot carrier solar cells and MEG. Conclusive evidence demonstrating an intrinsic phonon bottleneck in perovskites that is significantly stronger than GaAs has been demonstrated in perovskite nanoparticles. Extraction of hot carriers with selective contacts has been reported and its applicability to extremely thin absorber and concentrator solar cells proposed. Similarly, MEG with thresholds as low as 2.25 E_g, significantly better than conventional inorganic QDs, indicates that conversion efficiencies up to 44% are possible. Although slow-hot carrier cooling and CM have been convincingly outlined solar cells leveraging these exotic phenomena are not on the horizon yet; and approaches for operational hot-carrier and / or MEG photovoltaic devices still needs to be demonstrated. Nonadiabatic molecular dynamics simulations [224] and ultrafast measurements [225] have indicated that slower hot carrier relaxation can be

significantly modulated by the A site cation dynamics which affect the atomic displacements in the Pb−I framework and hence the electron−phonon couplings. Thus, cation mixing and engineering both in a nanostructured morphology as well as in the layered perovskite form can be avenues to control the hot-carrier cooling process. From a device point of view, an intermediate step towards the development of a hot-carrier solar cell would be the demonstration of a hot-carrier photodetector. Halide perovskite nanoparticles can also be employed in architectures where photodetectors beyond the bandgap limit operate due to the injection of hot carriers into a semiconductor structure to interact with cold carriers and excite them into higher energy states [226].

The utility of nanostructuring the halide perovskites for improved LEDs is very clear. Formation of nanograins and the confinement effect of MQW's in RP perovskites is reported to increase radiative recombination. Perovskite NCs have also been reported to yield the highest PLQY and the carrier cascade phenomena enabled by energy distribution, in NCs and RP phases, has been shown to be an important avenue for improving performance. Perovskite nanostructures as gain media also show very strong promise through quantum confinement and also through acting as natural optical microcavities yielding low threshold lasing and high quality factors.

Harnessing these advantages in electrically driven device configurations also require the management of charge transport and injection into the active perovskite layers. Approaches to reduce the insulating effects of the ligands to improve interparticle coupling by molecular metal chalcogenide complexes have been employed in colloidal quantum dots [227]. Adopting a similar approach for perovskite nanoparticles would require addressing the twin challenges of ligand charge and solvent polarity. Approaches that involve the growth of secondary perovskite layer around the active halide perovskite layer are also promising in addition to unlocking novel properties [27, 228]. Approaches that result in the *in-situ* formation of the nanograin morphology may also be promising, and requires more examination.

In addition to ambient and chemical stability, stability of the ionic halide perovskite semiconductors under applied electric field also needs to be addressed. Multiple studies have demonstrated that both 'A' site cation and halide ions have a tendency to move under the applied electric field. Such effects have been ascribed as some of the reasons behind hysteresis in photovoltaics, and have been beneficially utilized in neuromorphic devices. Ionic diffusion effects need to be controlled for long term operation of halide perovskite optoelectronic

devices. Recent findings which indicate that nanoparticles seem to have reduced ionic diffusion effects are promising in this regard [66].

As indicated earlier, the halide perovskite nanoparticles show excellent multiphoton absorption, with five-photon action cross-sections that are nine orders larger than the best reported organic molecules. The high multiphoton absorption properties of the nanoparticles can be utilized to form ultrafast photodetectors, which can exploit the nonlinear dependence of the photocurrent on the incident light intensity. This non-linear optical absorption property can also be utilized in a wide variety of bio-imaging applications due to the high penetration depth of low energy photons in biological systems. However, such applications are hampered by the incompatibility of the halide perovskite nanoparticle systems with aqueous conditions. Silica (SiO_2) is considered chemically stable and transparent, and would act to protect the perovskite NPs while not obstructing their optical properties. Such shelled NPs can also be utilized as downconverters in combination with conventional light sources. Similar approaches can be developed with conductive / semiconductive inorganic shells to extend their applications into electronic devices where the halide perovskites constitute the active layer. Such inorganic shells also allow for localization of the Pb content in perovskites, thus addressing toxicity concerns.

Continuous-wave or electrically excited lasing need further attention to improve its thermal stability, achieve large carrier mobility and density to reduce resistive heat losses. Lasing as well as high quality light emission in the blue region is additionally of great interest, especially with an eye towards full spectrum emission. The utilization of chloride as the halogen results in perovskites with large bandgaps, however the defect densities in these systems seem to preclude their utility in blue emitting devices. Additional challenges include phase segregation induced by ion movement under illumination and under biasing in the mixed halide system.

Bandgap tuning by utilizing quantization from nanocrystals or multi-layered perovskite on the other hand can offer alternatives pathways towards colour stable LEDs. Further modulation of colour and performance attributes of the perovskite nanostructures can be done by combining both the confinement effects described herein, viz. layered perovskites in nanostructured form. An interesting approach in this regard is the creation of exfoliates which are akin to the molecular analogues of graphene in RP perovskites [229, 230]. Initial results have already indicated that they can form a rich avenue of research, which will require scalable methodologies for exfoliation and synthesis [231, 232]. Light emitting transistors (LETs) have great relevance for displays as well as LEDs and electrically driven lasing. Although initial

results have been promising, ionic conduction is considered to be one of the limiting factors in its progress and nanostructuring will be one of the avenues to be considered here as well.

The achievements of metal halide perovskites in yielding record solar cell efficiencies, quantum yields, and optoelectronic tunability, all in solution processed form, is rapidly moving these semiconductors from academic research to being considered for industrialisation. Incorporation of organic cations and surface ligands enable formation of quasi-2D perovskites as well as nanocrystals that stretch six orders of magnitude from 0D quantum dots to 3D single crystals. These formulations permit access to phenomena of quantum confinement, tuning of band gaps, stability, and modulation of exciton dynamics. Chemical moieties and structural variants further accentuate the manifold synergy between localized quantum confinement, and long-range carrier dynamics. These phenomena that manifest themselves from atomic scale to device applications are well placed to challenge the performance limits and augur exciting attributes for nanostructured perovskite optoelectronics devices.

Conflicts of interest: There are no conflicts to declare.

Acknowledgements

This research was supported by the National Research Foundation, Prime Minister's Office, Singapore under its Competitive Research Programme (CRP Award No. NRF-CRP14-2014-03) and through the Singapore–Berkeley Research Initiative for Sustainable Energy (SinBeRISE) CREATE Program. Authors would like to thank Dr. Leow Shin Woei, Dr. Chin Xin Yu, Mr Biplab Ghosh, Mr Riyas Ahmad, Mr Abhijith Surendran and Dr John Rohit Abraham for their discussion and valuable comments during the preparation of this manuscript.

References

[1] Z. Li, T.R. Klein, D.H. Kim, M. Yang, J.J. Berry, M.F. van Hest, K. Zhu. Scalable fabrication of perovskite solar cells, Nature Reviews Materials 3(4) (2018) 18017.

[2] J.-P. Correa-Baena, A. Abate, M. Saliba, W. Tress, T.J. Jacobsson, M. Grätzel, A. Hagfeldt. The rapid evolution of highly efficient perovskite solar cells, Energy & Environmental Science 10(3) (2017) 710-727.

[3] https://www.nrel.gov/pv/cell-efficiency.html.

[4] L.C. Schmidt, A. Pertegás, S. González-Carrero, O. Malinkiewicz, S. Agouram, G. Mínguez Espallargas, H.J. Bolink, R.E. Galian, J. Pérez-Prieto. Nontemplate Synthesis of $CH_3NH_3PbBr_3$ Perovskite Nanoparticles, Journal of the American Chemical Society 136(3) (2014) 850-853.

[5] Z.-K. Tan, R.S. Moghaddam, M.L. Lai, P. Docampo, R. Higler, F. Deschler, M. Price, A. Sadhanala, L.M. Pazos, D. Credgington, F. Hanusch, T. Bein, H.J. Snaith, R.H. Friend. Bright light-emitting diodes based on organometal halide perovskite, Nature Nanotechnology 9 (2014) 687.

[6] G. Xing, N. Mathews, S.S. Lim, N. Yantara, X. Liu, D. Sabba, M. Grätzel, S. Mhaisalkar, T.C. Sum. Low-temperature solution-processed wavelength-tunable perovskites for lasing, Nature Materials 13 (2014) 476.

[7] G.G. Paschos, N. Somaschi, S.I. Tsintzos, D. Coles, J.L. Bricks, Z. Hatzopoulos, D.G. Lidzey, P.G. Lagoudakis, P.G. Savvidis. Hybrid organic-inorganic polariton laser, Scientific Reports 7(1) (2017) 11377.

[8] S. Chakraborty, W. Xie, N. Mathews, M. Sherburne, R. Ahuja, M. Asta, S.G. Mhaisalkar. Rational Design: A High-Throughput Computational Screening and Experimental Validation Methodology for Lead-Free and Emergent Hybrid Perovskites, ACS Energy Letters 2(4) (2017) 837-845.

[9] L. Mao, W. Ke, L. Pedesseau, Y. Wu, C. Katan, J. Even, M.R. Wasielewski, C.C. Stoumpos, M.G. Kanatzidis. Hybrid Dion–Jacobson 2D Lead Iodide Perovskites, Journal of the American Chemical Society 140(10) (2018) 3775-3783.

[10] B.-E. Cohen, Y. Li, Q. Meng, L. Etgar. Dion–Jacobson Two-Dimensional Perovskite Solar Cells Based on Benzene Dimethanammonium Cation, Nano Letters 19(4) (2019) 2588-2597.

[11] N. Yantara, A. Bruno, A. Iqbal, N.F. Jamaludin, C. Soci, S. Mhaisalkar, N. Mathews. Designing Efficient Energy Funneling Kinetics in Ruddlesden–Popper Perovskites for High-Performance Light-Emitting Diodes, Advanced Materials 30(33) (2018) 1800818.

[12] N. Wang, L. Cheng, R. Ge, S. Zhang, Y. Miao, W. Zou, C. Yi, Y. Sun, Y. Cao, R. Yang. Perovskite light-emitting diodes based on solution-processed self-organized multiple quantum wells, Nature Photonics 10(11) (2016) 699.

[13] M. Yuan, L.N. Quan, R. Comin, G. Walters, R. Sabatini, O. Voznyy, S. Hoogland, Y. Zhao, E.M. Beauregard, P. Kanjanaboos, Z. Lu, D.H. Kim, E.H. Sargent. Perovskite energy funnels for efficient light-emitting diodes, Nature Nanotechnology 11 (2016) 872.

[14] M. Li, Q. Wei, S.K. Muduli, N. Yantara, Q. Xu, N. Mathews, S.G. Mhaisalkar, G. Xing, T.C. Sum. Enhanced Exciton and Photon Confinement in Ruddlesden–Popper Perovskite

Microplatelets for Highly Stable Low-Threshold Polarized Lasing, Advanced Materials 30(23) (2018) 1707235.

[15] E.M. Sanehira, A.R. Marshall, J.A. Christians, S.P. Harvey, P.N. Ciesielski, L.M. Wheeler, P. Schulz, L.Y. Lin, M.C. Beard, J.M. Luther. Enhanced mobility $CsPbI_3$ quantum dot arrays for record-efficiency, high-voltage photovoltaic cells, Science Advances 3(10) (2017).

[16] Y.-H. Kim, G.-H. Lee, Y.-T. Kim, C. Wolf, H.J. Yun, W. Kwon, C.G. Park, T.W. Lee. High efficiency perovskite light-emitting diodes of ligand-engineered colloidal formamidinium lead bromide nanoparticles, Nano Energy 38 (2017) 51-58.

[17] M.V. Kovalenko, L. Protesescu, M.I. Bodnarchuk. Properties and potential optoelectronic applications of lead halide perovskite nanocrystals, Science 358(6364) (2017) 745-750.

[18] A. Kostopoulou, E. Kymakis, E. Stratakis. Perovskite nanostructures for photovoltaic and energy storage devices, Journal of Materials Chemistry A 6(21) (2018) 9765-9798.

[19] T. Qiu, Y. Hu, F. Xu, Z. Yan, F. Bai, G. Jia, S. Zhang. Recent advances in one-dimensional halide perovskites for optoelectronic applications, Nanoscale 10(45) (2018) 20963-20989.

[20] Y.-H. Kim, H. Cho, T.-W. Lee. Metal halide perovskite light emitters, Proceedings of the National Academy of Sciences 113(42) (2016) 11694-11702.

[21] S.A. Veldhuis, P.P. Boix, N. Yantara, M. Li, T.C. Sum, N. Mathews, S.G. Mhaisalkar. Perovskite Materials for Light-Emitting Diodes and Lasers, Advanced Materials 28(32) (2016) 6804-6834.

[22] H. Lin, C. Zhou, Y. Tian, T. Siegrist, B. Ma. Low-Dimensional Organometal Halide Perovskites, ACS Energy Letters 3(1) (2018) 54-62.

[23] M. Li, S. Bhaumik, T.W. Goh, M.S. Kumar, N. Yantara, M. Grätzel, S. Mhaisalkar, N. Mathews, T.C. Sum. Slow cooling and highly efficient extraction of hot carriers in colloidal perovskite nanocrystals, Nature Communications 8 (2017) 14350.

[24] M. Li, R. Begum, J. Fu, Q. Xu, T.M. Koh, S.A. Veldhuis, M. Grätzel, N. Mathews, S. Mhaisalkar, T.C. Sum. Low threshold and efficient multiple exciton generation in halide perovskite nanocrystals, Nature Communications 9(1) (2018) 4197.

[25] C. de Weerd, L. Gomez, A. Capretti, D.M. Lebrun, E. Matsubara, J. Lin, M. Ashida, F.C.M. Spoor, L.D.A. Siebbeles, A.J. Houtepen, K. Suenaga, Y. Fujiwara, T. Gregorkiewicz. Efficient carrier multiplication in CsPbI3 perovskite nanocrystals, Nature Communications 9(1) (2018) 4199.

[26] X.Y. Chin, A. Perumal, A. Bruno, N. Yantara, S.A. Veldhuis, L. Martinez-Sarti, B. Chandran, V. Chirvony, A.S.-Z. Lo, J. So, C. Soci, M. Gratzel, H.J. Bolink, N. Mathews, S.G. Mhaisalkar. Self-assembled hierarchical nanostructured perovskites enable highly efficient LEDs via an energy cascade, Energy & Environmental Science 11 (2018) 1770-1778

[27] W. Chen, S. Bhaumik, S.A. Veldhuis, G. Xing, Q. Xu, M. Grätzel, S. Mhaisalkar, N. Mathews, T.C. Sum. Giant five-photon absorption from multidimensional core-shell halide perovskite colloidal nanocrystals, Nature Communications 8 (2017) 15198.

[28] Q. Zheng, H. Zhu, S.-C. Chen, C. Tang, E. Ma, X. Chen. Frequency-upconverted stimulated emission by simultaneous five-photon absorption, Nature Photonics 7 (2013) 234.

[29] Y. Ling, Z. Yuan, Y. Tian, X. Wang, J.C. Wang, Y. Xin, K. Hanson, B. Ma, H. Gao. Bright Light-Emitting Diodes Based on Organometal Halide Perovskite Nanoplatelets, Advanced Materials 28(2) (2016) 305-311.

[30] H. Zhu, Y. Fu, F. Meng, X. Wu, Z. Gong, Q. Ding, M.V. Gustafsson, M.T. Trinh, S. Jin, X. Zhu. Lead halide perovskite nanowire lasers with low lasing thresholds and high quality factors, Nature materials 14(6) (2015) 636.

[31] Y. Fu, H. Zhu, J. Chen, M.P. Hautzinger, X.Y. Zhu, S. Jin. Metal halide perovskite nanostructures for optoelectronic applications and the study of physical properties, Nature Reviews Materials 4(3) (2019) 169-188.

[32] Z. Tan, Y. Wu, H. Hong, J. Yin, J. Zhang, L. Lin, M. Wang, X. Sun, L. Sun, Y. Huang, K. Liu, Z. Liu, H. Peng. Two-Dimensional $(C_4H_9NH_3)_2PbBr_4$ Perovskite Crystals for High-Performance Photodetector, Journal of the American Chemical Society 138(51) (2016) 16612-16615.

[33] K.T. Cho, Y. Zhang, S. Orlandi, M. Cavazzini, I. Zimmermann, A. Lesch, N. Tabet, G. Pozzi, G. Grancini, M.K. Nazeeruddin. Water-Repellent Low-Dimensional Fluorous Perovskite as Interfacial Coating for 20% Efficient Solar Cells, Nano Letters 18(9) (2018) 5467-5474.

[34] B. Saparov, D.B. Mitzi. Organic–Inorganic Perovskites: Structural Versatility for Functional Materials Design, Chemical Reviews 116(7) (2016) 4558-4596.

[35] W. Li, Z. Wang, F. Deschler, S. Gao, R.H. Friend, A.K. Cheetham. Chemically diverse and multifunctional hybrid organic–inorganic perovskites, Nature Reviews Materials 2 (2017) 16099.

[36] E. Mosconi, P. Umari, F. De Angelis. Electronic and optical properties of MAPbX3 perovskites (X = I, Br, Cl): a unified DFT and GW theoretical analysis, Physical Chemistry Chemical Physics 18(39) (2016) 27158-27164.

[37] A. Amat, E. Mosconi, E. Ronca, C. Quarti, P. Umari, M.K. Nazeeruddin, M. Grätzel, F. De Angelis. Cation-Induced Band-Gap Tuning in Organohalide Perovskites: Interplay of Spin–Orbit Coupling and Octahedra Tilting, Nano Letters 14(6) (2014) 3608-3616.

[38] C.C. Stoumpos, C.D. Malliakas, M.G. Kanatzidis. Semiconducting Tin and Lead Iodide Perovskites with Organic Cations: Phase Transitions, High Mobilities, and Near-Infrared Photoluminescent Properties, Inorganic Chemistry 52(15) (2013) 9019-9038.

[39] J.S. Manser, J.A. Christians, P.V. Kamat. Intriguing Optoelectronic Properties of Metal Halide Perovskites, Chemical Reviews 116(21) (2016) 12956-13008.

[40] D.P. McMeekin, G. Sadoughi, W. Rehman, G.E. Eperon, M. Saliba, M.T. Hörantner, A. Haghighirad, N. Sakai, L. Korte, B. Rech, M.B. Johnston, L.M. Herz, H.J. Snaith. A mixed-cation lead mixed-halide perovskite absorber for tandem solar cells, Science 351(6269) (2016) 151-155.

[41] F. Hao, C.C. Stoumpos, R.P.H. Chang, M.G. Kanatzidis. Anomalous Band Gap Behavior in Mixed Sn and Pb Perovskites Enables Broadening of Absorption Spectrum in Solar Cells, Journal of the American Chemical Society 136(22) (2014) 8094-8099.

[42] M.R. Filip, G.E. Eperon, H.J. Snaith, F. Giustino. Steric engineering of metal-halide perovskites with tunable optical band gaps, Nature Communications 5 (2014) 5757.

[43] N. Pellet, P. Gao, G. Gregori, T.-Y. Yang, M.K. Nazeeruddin, J. Maier, M. Grätzel. Mixed-Organic-Cation Perovskite Photovoltaics for Enhanced Solar-Light Harvesting, Angewandte Chemie International Edition 53(12) (2014) 3151-3157.

[44] D.G. Billing, A. Lemmerer. Inorganic–organic hybrid materials incorporating primary cyclic ammonium cations: The lead iodide series, CrystEngComm 9(3) (2007) 236-244.

[45] T. Dammak, M. Koubaa, K. Boukheddaden, H. Bougzhala, A. Mlayah, Y. Abid. Two-Dimensional Excitons and Photoluminescence Properties of the Organic/Inorganic (4-FC6H4C2H4NH3)2[PbI4] Nanomaterial, The Journal of Physical Chemistry C 113(44) (2009) 19305-19309.

[46] L. Peng, A. Tang, C. Yang, F. Teng. Size-controlled synthesis of highly luminescent organometal halide perovskite quantum dots, Journal of Alloys and Compounds 687 (2016) 506-513.

[47] L. Protesescu, S. Yakunin, M.I. Bodnarchuk, F. Krieg, R. Caputo, C.H. Hendon, R.X. Yang, A. Walsh, M.V. Kovalenko. Nanocrystals of Cesium Lead Halide Perovskites (CsPbX3, X = Cl, Br, and I): Novel Optoelectronic Materials Showing Bright Emission with Wide Color Gamut, Nano Letters 15(6) (2015) 3692-3696.

[48] F. Liu, Y. Zhang, C. Ding, S. Kobayashi, T. Izuishi, N. Nakazawa, T. Toyoda, T. Ohta, S. Hayase, T. Minemoto, K. Yoshino, S. Dai, Q. Shen. Highly Luminescent Phase-Stable CsPbI3 Perovskite Quantum Dots Achieving Near 100% Absolute Photoluminescence Quantum Yield, ACS Nano 11(10) (2017) 10373-10383.

[49] K. Tanaka, T. Takahashi, T. Ban, T. Kondo, K. Uchida, N. Miura. Comparative study on the excitons in lead-halide-based perovskite-type crystals $CH_3NH_3PbBr_3$ $CH_3NH_3PbI_3$, Solid State Communications 127(9) (2003) 619-623.

[50] M. Hirasawa, T. Ishihara, T. Goto, K. Uchida, N. Miura. Magnetoabsorption of the lowest exciton in perovskite-type compound (CH3NH3)PbI3, Physica B: Condensed Matter 201 (1994) 427-430.

[51] T. Ishihara. Optical properties of PbI-based perovskite structures, Journal of Luminescence 60-61 (1994) 269-274.

[52] K. Wu, A. Bera, C. Ma, Y. Du, Y. Yang, L. Li, T. Wu. Temperature-dependent excitonic photoluminescence of hybrid organometal halide perovskite films, Physical Chemistry Chemical Physics 16(41) (2014) 22476-22481.

[53] R.J. Elliott. Intensity of Optical Absorption by Excitons, Physical Review 108(6) (1957) 1384-1389.

[54] J. Even, L. Pedesseau, C. Katan. Analysis of Multivalley and Multibandgap Absorption and Enhancement of Free Carriers Related to Exciton Screening in Hybrid Perovskites, The Journal of Physical Chemistry C 118(22) (2014) 11566-11572.

[55] M. Saba, M. Cadelano, D. Marongiu, F. Chen, V. Sarritzu, N. Sestu, C. Figus, M. Aresti, R. Piras, A. Geddo Lehmann, C. Cannas, A. Musinu, F. Quochi, A. Mura, G. Bongiovanni. Correlated electron–hole plasma in organometal perovskites, Nature Communications 5 (2014) 5049.

[56] C. Wehrenfennig, G.E. Eperon, M.B. Johnston, H.J. Snaith, L.M. Herz. High Charge Carrier Mobilities and Lifetimes in Organolead Trihalide Perovskites, Advanced Materials 26(10) (2014) 1584-1589.

[57] S.D. Stranks, G.E. Eperon, G. Grancini, C. Menelaou, M.J.P. Alcocer, T. Leijtens, L.M. Herz, A. Petrozza, H.J. Snaith. Electron-Hole Diffusion Lengths Exceeding 1 Micrometer in an Organometal Trihalide Perovskite Absorber, Science 342(6156) (2013) 341-344.

[58] M. Hirasawa, T. Ishihara, T. Goto. Exciton Features in 0-, 2-, and 3-Dimensional Networks of [PbI6]4- Octahedra, Journal of the Physical Society of Japan 63(10) (1994) 3870-3879.

[59] E. Hanamura, N. Nagaosa, M. Kumagai, T. Takagahara. Quantum wells with enhanced exciton effects and optical non-linearity, Materials Science and Engineering: B 1(3) (1988) 255-258.

[60] S. Elleuch, T. Dammak, Y. Abid, A. Mlayah, H. Boughzala. Synthesis, structural and optical properties of a novel bilayered organic–inorganic perovskite $C_5Pb_2I_5$, Journal of Luminescence 130(4) (2010) 531-535.

[61] T. Ishihara, J. Takahashi, T. Goto. Optical properties due to electronic transitions in two-dimensional semiconductors $(C_nH_{2n+1}NH_3)_2PbI_4$, Physical Review B 42(17) (1990) 11099-11107.

[62] X. Wu, M.T. Trinh, X.Y. Zhu. Excitonic Many-Body Interactions in Two-Dimensional Lead Iodide Perovskite Quantum Wells, The Journal of Physical Chemistry C 119(26) (2015) 14714-14721.

[63] K. Ema, M. Inomata, Y. Kato, H. Kunugita, M. Era. Nearly Perfect Triplet-Triplet Energy Transfer from Wannier Excitons to Naphthalene in Organic-Inorganic Hybrid Quantum-Well Materials, Physical Review Letters 100(25) (2008) 257401.

[64] V.M. Agranovich, Y.N. Gartstein, M. Litinskaya. Hybrid Resonant Organic–Inorganic Nanostructures for Optoelectronic Applications, Chemical Reviews 111(9) (2011) 5179-5214.

[65] S.A. Kulkarni, S. Muduli, G. Xing, N. Yantara, M. Li, S. Chen, T.C. Sum, N. Mathews, T.J. White, S.G. Mhaisalkar. Modulating Excitonic Recombination Effects through One-Step Synthesis of Perovskite Nanoparticles for Light-Emitting Diodes, ChemSusChem 10(19) (2017) 3818-3824.

[66] Y.-H. Kim, C. Wolf, H. Kim, T.-W. Lee. Charge carrier recombination and ion migration in metal-halide perovskite nanoparticle films for efficient light-emitting diodes, Nano Energy 52 (2018) 329-335.

[67] K. Zheng, Q. Zhu, M. Abdellah, M.E. Messing, W. Zhang, A. Generalov, Y. Niu, L. Ribaud, S.E. Canton, T. Pullerits. Exciton Binding Energy and the Nature of Emissive States in Organometal Halide Perovskites, The Journal of Physical Chemistry Letters 6(15) (2015) 2969-2975.

[68] J. Li, L. Luo, H. Huang, C. Ma, Z. Ye, J. Zeng, H. He. 2D Behaviors of Excitons in Cesium Lead Halide Perovskite Nanoplatelets, The Journal of Physical Chemistry Letters 8(6) (2017) 1161-1168.

[69] J.A. Sichert, Y. Tong, N. Mutz, M. Vollmer, S. Fischer, K.Z. Milowska, R. García Cortadella, B. Nickel, C. Cardenas-Daw, J.K. Stolarczyk, A.S. Urban, J. Feldmann. Quantum Size Effect in Organometal Halide Perovskite Nanoplatelets, Nano Letters 15(10) (2015) 6521-6527.

[70] O. Yaffe, A. Chernikov, Z.M. Norman, Y. Zhong, A. Velauthapillai, A. van der Zande, J.S. Owen, T.F. Heinz. Excitons in ultrathin organic-inorganic perovskite crystals, Physical Review B 92(4) (2015) 045414.

[71] M.B. Johnston, L.M. Herz. Hybrid Perovskites for Photovoltaics: Charge-Carrier Recombination, Diffusion, and Radiative Efficiencies, Accounts of Chemical Research 49(1) (2016) 146-154.

[72] C.M. Sutter-Fella, Y. Li, M. Amani, J.W. Ager, F.M. Toma, E. Yablonovitch, I.D. Sharp, A. Javey. High Photoluminescence Quantum Yield in Band Gap Tunable Bromide Containing Mixed Halide Perovskites, Nano Letters 16(1) (2016) 800-806.

[73] J. Huang, Y. Yuan, Y. Shao, Y. Yan. Understanding the physical properties of hybrid perovskites for photovoltaic applications, Nature Reviews Materials 2 (2017) 17042.

[74] G. Xing, B. Wu, X. Wu, M. Li, B. Du, Q. Wei, J. Guo, E.K.L. Yeow, T.C. Sum, W. Huang. Transcending the slow bimolecular recombination in lead-halide perovskites for electroluminescence, Nature Communications 8 (2017) 14558.

[75] I.B. Koutselas, L. Ducasse, G.C. Papavassiliou. Electronic properties of three- and low-dimensional semiconducting materials with Pb halide and Sn halide units, Journal of Physics: Condensed Matter 8(9) (1996) 1217.

[76] M.C. Gélvez-Rueda, E.M. Hutter, D.H. Cao, N. Renaud, C.C. Stoumpos, J.T. Hupp, T.J. Savenije, M.G. Kanatzidis, F.C. Grozema. Interconversion between Free Charges and Bound Excitons in 2D Hybrid Lead Halide Perovskites, The Journal of Physical Chemistry C 121(47) (2017) 26566-26574.

[77] W. Zou, R. Li, S. Zhang, Y. Liu, N. Wang, Y. Cao, Y. Miao, M. Xu, Q. Guo, D. Di, L. Zhang, C. Yi, F. Gao, R.H. Friend, J. Wang, W. Huang. Minimising efficiency roll-off in high-brightness perovskite light-emitting diodes, Nature Communications 9(1) (2018) 608.

[78] M. Ban, Y. Zou, J.P.H. Rivett, Y. Yang, T.H. Thomas, Y. Tan, T. Song, X. Gao, D. Credington, F. Deschler, H. Sirringhaus, B. Sun. Solution-processed perovskite light emitting diodes with efficiency exceeding 15% through additive-controlled nanostructure tailoring, Nature Communications 9(1) (2018) 3892.

[79] A. Swarnkar, A.R. Marshall, E.M. Sanehira, B.D. Chernomordik, D.T. Moore, J.A. Christians, T. Chakrabarti, J.M. Luther. Quantum dot–induced phase stabilization of α-CsPbI₃ perovskite for high-efficiency photovoltaics, Science 354(6308) (2016) 92-95.

[80] X. Zhang, R. Munir, Z. Xu, Y. Liu, H. Tsai, W. Nie, J. Li, T. Niu, D.-M. Smilgies, M.G. Kanatzidis, A.D. Mohite, K. Zhao, A. Amassian, S. Liu. Phase Transition Control for High Performance Ruddlesden–Popper Perovskite Solar Cells, Advanced Materials 30(21) (2018) 1707166.

[81] A. Rao, R.H. Friend. Harnessing singlet exciton fission to break the Shockley–Queisser limit, Nature Reviews Materials 2 (2017) 17063.

[82] C. Battaglia, A. Cuevas, S. De Wolf. High-efficiency crystalline silicon solar cells: status and perspectives, Energy & Environmental Science 9(5) (2016) 1552-1576.

[83] M.A. Green. Radiative efficiency of state-of-the-art photovoltaic cells, Progress in Photovoltaics: Research and Applications 20(4) (2012) 472-476.

[84] O.D. Miller, E. Yablonovitch, S.R. Kurtz. Strong Internal and External Luminescence as Solar Cells Approach the Shockley–Queisser Limit, IEEE Journal of Photovoltaics 2(3) (2012) 303-311.

[85] A.J. Nozik. Spectroscopy and hot electron relaxation dynamics in semiconductor quantum well and quantum dots Annual Review of Physical Chemistry 52(1) (2001) 193-231.

[86] M.A. Green. Third generation photovoltaics: Ultra-high conversion efficiency at low cost, Progress in Photovoltaics: Research and Applications 9(2) (2001) 123-135.

[87] P. Papagiorgis, L. Protesescu, M.V. Kovalenko, A. Othonos, G. Itskos. Long-Lived Hot Carriers in Formamidinium Lead Iodide Nanocrystals, The Journal of Physical Chemistry C 121(22) (2017) 12434-12440.

[88] Z. Guo, Y. Wan, M. Yang, J. Snaider, K. Zhu, L. Huang. Long-range hot-carrier transport in hybrid perovskites visualized by ultrafast microscopy, Science 356(6333) (2017) 59-62.

[89] D. König, K. Casalenuovo, Y. Takeda, G. Conibeer, J.F. Guillemoles, R. Patterson, L.M. Huang, M.A. Green. Hot carrier solar cells: Principles, materials and design, Physica E: Low-dimensional Systems and Nanostructures 42(10) (2010) 2862-2866.

[90] R.D. Schaller, V.I. Klimov. High Efficiency Carrier Multiplication in PbSe Nanocrystals: Implications for Solar Energy Conversion, Physical Review Letters 92(18) (2004) 186601.

[91] Y. Yan, R.W. Crisp, J. Gu, B.D. Chernomordik, G.F. Pach, Ashley R. Marshall, J.A. Turner, M.C. Beard. Multiple exciton generation for photoelectrochemical hydrogen evolution reactions with quantum yields exceeding 100%, Nature Energy 2 (2017) 17052.

[92] H. Eshet, R. Baer, D. Neuhauser, E. Rabani. Theory of highly efficient multiexciton generation in type-II nanorods, Nature Communications 7 (2016) 13178.

[93] D.J. Vogel, A. Kryjevski, T. Inerbaev, D.S. Kilin. Photoinduced Single- and Multiple-Electron Dynamics Processes Enhanced by Quantum Confinement in Lead Halide Perovskite Quantum Dots, The Journal of Physical Chemistry Letters 8(13) (2017) 3032-3039.

[94] J.A. McGuire, J. Joo, J.M. Pietryga, R.D. Schaller, V.I. Klimov. New Aspects of Carrier Multiplication in Semiconductor Nanocrystals, Accounts of Chemical Research 41(12) (2008) 1810-1819.

[95] D.H. Cao, C.C. Stoumpos, O.K. Farha, J.T. Hupp, M.G. Kanatzidis. 2D Homologous Perovskites as Light-Absorbing Materials for Solar Cell Applications, Journal of the American Chemical Society 137(24) (2015) 7843-7850.

[96] I.C. Smith, E.T. Hoke, D. Solis-Ibarra, M.D. McGehee, H.I. Karunadasa. A Layered Hybrid Perovskite Solar-Cell Absorber with Enhanced Moisture Stability, Angewandte Chemie International Edition 53(42) (2014) 11232-11235.

[97] L.N. Quan, M. Yuan, R. Comin, O. Voznyy, E.M. Beauregard, S. Hoogland, A. Buin, A.R. Kirmani, K. Zhao, A. Amassian, D.H. Kim, E.H. Sargent. Ligand-Stabilized Reduced-Dimensionality Perovskites, Journal of the American Chemical Society 138(8) (2016) 2649-2655.

[98] G. Grancini, C. Roldán-Carmona, I. Zimmermann, E. Mosconi, X. Lee, D. Martineau, S. Narbey, F. Oswald, F. De Angelis, M. Graetzel, M.K. Nazeeruddin. One-Year stable perovskite solar cells by 2D/3D interface engineering, Nature Communications 8 (2017) 15684.

[99] Q. Wang, J. Ren, X.-F. Peng, X.-X. Ji, X.-H. Yang. Efficient Sky-Blue Perovskite Light-Emitting Devices Based on Ethylammonium Bromide Induced Layered Perovskites, ACS Applied Materials & Interfaces 9(35) (2017) 29901-29906.

[100] T.M. Koh, V. Shanmugam, J. Schlipf, L. Oesinghaus, P. Müller-Buschbaum, N. Ramakrishnan, V. Swamy, N. Mathews, P.P. Boix, S.G. Mhaisalkar. Nanostructuring Mixed-Dimensional Perovskites: A Route Toward Tunable, Efficient Photovoltaics, Advanced Materials 28(19) (2016) 3653-3661.

[101] A.Z. Chen, M. Shiu, J.H. Ma, M.R. Alpert, D. Zhang, B.J. Foley, D.-M. Smilgies, S.-H. Lee, J.J. Choi. Origin of vertical orientation in two-dimensional metal halide perovskites and its effect on photovoltaic performance, Nature Communications 9(1) (2018) 1336.

[102] J.-C. Blancon, H. Tsai, W. Nie, C.C. Stoumpos, L. Pedesseau, C. Katan, M. Kepenekian, C.M.M. Soe, K. Appavoo, M.Y. Sfeir, S. Tretiak, P.M. Ajayan, M.G. Kanatzidis, J. Even, J.J. Crochet, A.D. Mohite. Extremely efficient internal exciton dissociation through edge states in layered 2D perovskites, Science 355(6331) (2017) 1288-1292.

[103] J. Liu, J. Leng, K. Wu, J. Zhang, S. Jin. Observation of Internal Photoinduced Electron and Hole Separation in Hybrid Two-Dimentional Perovskite Films, Journal of the American Chemical Society 139(4) (2017) 1432-1435.

[104] C.C. Stoumpos, C.M.M. Soe, H. Tsai, W. Nie, J.-C. Blancon, D.H. Cao, F. Liu, B. Traoré, C. Katan, J. Even, A.D. Mohite, M.G. Kanatzidis. High Members of the 2D Ruddlesden-Popper Halide Perovskites: Synthesis, Optical Properties, and Solar Cells of $(CH_3(CH_2)_3NH_3)_2(CH_3NH_3)_4Pb_5I_{16}$, Chem 2(3) (2017) 427-440.

[105] T.M. Koh, V. Shanmugam, X. Guo, S.S. Lim, O. Filonik, E.M. Herzig, P. Müller-Buschbaum, V. Swamy, S.T. Chien, S.G. Mhaisalkar, N. Mathews. Enhancing moisture tolerance in efficient hybrid 3D/2D perovskite photovoltaics, Journal of Materials Chemistry A 6(5) (2018) 2122-2128.

[106] P. Chen, Y. Bai, S. Wang, M. Lyu, J.-H. Yun, L. Wang. In Situ Growth of 2D Perovskite Capping Layer for Stable and Efficient Perovskite Solar Cells, Advanced Functional Materials 28(17) (2018) 1706923.

[107] K.T. Cho, G. Grancini, Y. Lee, E. Oveisi, J. Ryu, O. Almora, M. Tschumi, P.A. Schouwink, G. Seo, S. Heo, J. Park, J. Jang, S. Paek, G. Garcia-Belmonte, M.K. Nazeeruddin. Selective growth of layered perovskites for stable and efficient photovoltaics, Energy & Environmental Science 11(4) (2018) 952-959.

[108] T.M. Koh, J. Huang, I. Neogi, P.P. Boix, S.G. Mhaisalkar, N. Mathews. High Stability Bilayered Perovskites through Crystallization Driven Self-Assembly, ACS Applied Materials & Interfaces 9(34) (2017) 28743-28749.

[109] L. Etgar. The merit of perovskite's dimensionality; can this replace the 3D halide perovskite?, Energy & Environmental Science 11(2) (2018) 234-242.

[110] B. Conings, J. Drijkoningen, N. Gauquelin, A. Babayigit, J. D'Haen, L. D'Olieslaeger, A. Ethirajan, J. Verbeeck, J. Manca, E. Mosconi, F.D. Angelis, H.-G. Boyen. Intrinsic Thermal Instability of Methylammonium Lead Trihalide Perovskite, Advanced Energy Materials 5(15) (2015) 1500477.

[111] R.J. Sutton, G.E. Eperon, L. Miranda, E.S. Parrott, B.A. Kamino, J.B. Patel, M.T. Hörantner, M.B. Johnston, A.A. Haghighirad, D.T. Moore, H.J. Snaith. Bandgap-Tunable

Cesium Lead Halide Perovskites with High Thermal Stability for Efficient Solar Cells, Advanced Energy Materials 6(8) (2016) 1502458.

[112] R.E. Beal, D.J. Slotcavage, T. Leijtens, A.R. Bowring, R.A. Belisle, W.H. Nguyen, G.F. Burkhard, E.T. Hoke, M.D. McGehee. Cesium Lead Halide Perovskites with Improved Stability for Tandem Solar Cells, The Journal of Physical Chemistry Letters 7(5) (2016) 746-751.

[113] J.-H. Im, J. Luo, M. Franckevičius, N. Pellet, P. Gao, T. Moehl, S.M. Zakeeruddin, M.K. Nazeeruddin, M. Grätzel, N.-G. Park. Nanowire Perovskite Solar Cell, Nano Letters 15(3) (2015) 2120-2126.

[114] A.F. Gualdrón-Reyes, S.J. Yoon, I. Mora-Seró. Recent insights for achieving mixed halide perovskites without halide segregation, Current Opinion in Electrochemistry 11 (2018) 84-90.

[115] P. Kour, M.C. Reddy, R. Naphade, S. Ogale. Quaternary alkylammonium salt incorporated 2D/3D mixed halide perovskite with highly enhanced photoluminescence and arrested iodide/bromide phase segregation, APL Materials 6(8) (2018) 086107.

[116] S. Draguta, O. Sharia, S.J. Yoon, M.C. Brennan, Y.V. Morozov, J.S. Manser, P.V. Kamat, W.F. Schneider, M. Kuno. Rationalizing the light-induced phase separation of mixed halide organic–inorganic perovskites, Nature Communications 8(1) (2017) 200.

[117] Y. Cao, N. Wang, H. Tian, J. Guo, Y. Wei, H. Chen, Y. Miao, W. Zou, K. Pan, Y. He, H. Cao, Y. Ke, M. Xu, Y. Wang, M. Yang, K. Du, Z. Fu, D. Kong, D. Dai, Y. Jin, G. Li, H. Li, Q. Peng, J. Wang, W. Huang. Perovskite light-emitting diodes based on spontaneously formed submicrometre-scale structures, Nature 562(7726) (2018) 249-253.

[118] K. Lin, J. Xing, L.N. Quan, F.P.G. de Arquer, X. Gong, J. Lu, L. Xie, W. Zhao, D. Zhang, C. Yan, W. Li, X. Liu, Y. Lu, J. Kirman, E.H. Sargent, Q. Xiong, Z. Wei. Perovskite light-emitting diodes with external quantum efficiency exceeding 20 per cent, Nature 562(7726) (2018) 245-248.

[119] T. Chiba, Y. Hayashi, H. Ebe, K. Hoshi, J. Sato, S. Sato, Y.-J. Pu, S. Ohisa, J. Kido. Anion-exchange red perovskite quantum dots with ammonium iodine salts for highly efficient light-emitting devices, Nature Photonics 12(11) (2018) 681-687.

[120] S.D. Stranks, V.M. Burlakov, T. Leijtens, J.M. Ball, A. Goriely, H.J. Snaith. Recombination Kinetics in Organic-Inorganic Perovskites: Excitons, Free Charge, and Subgap States, Physical Review Applied 2(3) (2014) 034007.

[121] X. Wu, M.T. Trinh, D. Niesner, H. Zhu, Z. Norman, J.S. Owen, O. Yaffe, B.J. Kudisch, X.Y. Zhu. Trap States in Lead Iodide Perovskites, Journal of the American Chemical Society 137(5) (2015) 2089-2096.

[122] T.J. Savenije, C.S. Ponseca, L. Kunneman, M. Abdellah, K. Zheng, Y. Tian, Q. Zhu, S.E. Canton, I.G. Scheblykin, T. Pullerits, A. Yartsev, V. Sundström. Thermally Activated Exciton Dissociation and Recombination Control the Carrier Dynamics in Organometal Halide Perovskite, The Journal of Physical Chemistry Letters 5(13) (2014) 2189-2194.

[123] Z.-K. Tan, R.S. Moghaddam, M.L. Lai, P. Docampo, R. Higler, F. Deschler, M. Price, A. Sadhanala, L.M. Pazos, D. Credgington, F. Hanusch, T. Bein, H.J. Snaith, R.H. Friend. Bright light-emitting diodes based on organometal halide perovskite, Nat Nano 9(9) (2014) 687-692.

[124] M. Era, S. Morimoto, T. Tsutsui, S. Saito. Organic-inorganic heterostructure electroluminescent device using a layered perovskite semiconductor $(C_6H_5C_2H_4NH_3)_2PbI_4$, Applied Physics Letters 65(6) (1994) 676-678.

[125] T. Hattori, T. Taira, M. Era, T. Tsutsui, S. Saito. Highly efficient electroluminescence from a heterostructure device combined with emissive layered-perovskite and an electron-transporting organic compound, Chemical Physics Letters 254(1) (1996) 103-108.

[126] K. Tvingstedt, O. Malinkiewicz, A. Baumann, C. Deibel, H.J. Snaith, V. Dyakonov, H.J. Bolink. Radiative efficiency of lead iodide based perovskite solar cells, Scientific Reports 4 (2014) 6071.

[127] H. Cho, S.-H. Jeong, M.-H. Park, Y.-H. Kim, C. Wolf, C.-L. Lee, J.H. Heo, A. Sadhanala, N. Myoung, S. Yoo, S.H. Im, R.H. Friend, T.-W. Lee. Overcoming the electroluminescence efficiency limitations of perovskite light-emitting diodes, Science 350(6265) (2015) 1222-1225.

[128] G. Li, Z.-K. Tan, D. Di, M.L. Lai, L. Jiang, J.H.-W. Lim, R.H. Friend, N.C. Greenham. Efficient Light-Emitting Diodes Based on Nanocrystalline Perovskite in a Dielectric Polymer Matrix, Nano Letters 15(4) (2015) 2640-2644.

[129] J.-W. Lee, Y.J. Choi, J.-M. Yang, S. Ham, S.K. Jeon, J.Y. Lee, Y.-H. Song, E.K. Ji, D.-H. Yoon, S. Seo, H. Shin, G.S. Han, H.S. Jung, D. Kim, N.-G. Park. In-Situ Formed Type I Nanocrystalline Perovskite Film for Highly Efficient Light-Emitting Diode, ACS Nano 11(3) (2017) 3311-3319.

[130] Y.H. Kim, H. Cho, J.H. Heo, T.S. Kim, N. Myoung, C.L. Lee, S.H. Im, T.W. Lee. Multicolored Organic/Inorganic Hybrid Perovskite Light-Emitting Diodes, Advanced Materials 27(7) (2015) 1248-1254.

[131] J. Byun, H. Cho, C. Wolf, M. Jang, A. Sadhanala, R.H. Friend, H. Yang, T.W. Lee. Efficient Visible Quasi-2D Perovskite Light-Emitting Diodes, Advanced Materials 28(34) (2016) 7515-7520.

[132] Y.F. Ng, S.A. Kulkarni, S. Parida, N.F. Jamaludin, N. Yantara, A. Bruno, C. Soci, S. Mhaisalkar, N. Mathews. Highly efficient Cs-based perovskite light-emitting diodes enabled by energy funnelling, Chemical Communications 53(88) (2017) 12004-12007.

[133] L. Zhao, Y.-W. Yeh, N.L. Tran, F. Wu, Z. Xiao, R.A. Kerner, Y.L. Lin, G.D. Scholes, N. Yao, B.P. Rand. In Situ Preparation of Metal Halide Perovskite Nanocrystal Thin Films for Improved Light-Emitting Devices, ACS Nano 11(4) (2017) 3957-3964.

[134] H. Wang, X. Zhang, Q. Wu, F. Cao, D. Yang, Y. Shang, Z. Ning, W. Zhang, W. Zheng, Y. Yan, S.V. Kershaw, L. Zhang, A.L. Rogach, X. Yang. Trifluoroacetate induced small-grained $CsPbBr_3$ perovskite films result in efficient and stable light-emitting devices, Nature Communications 10(1) (2019) 665.

[135] X. Yang, X. Zhang, J. Deng, Z. Chu, Q. Jiang, J. Meng, P. Wang, L. Zhang, Z. Yin, J. You. Efficient green light-emitting diodes based on quasi-two-dimensional composition and phase engineered perovskite with surface passivation, Nature Communications 9(1) (2018) 570.

[136] Q.A. Akkerman, V. D'Innocenzo, S. Accornero, A. Scarpellini, A. Petrozza, M. Prato, L. Manna. Tuning the Optical Properties of Cesium Lead Halide Perovskite Nanocrystals by

Anion Exchange Reactions, Journal of the American Chemical Society 137(32) (2015) 10276-10281.

[137] A. Sadhanala, S. Ahmad, B. Zhao, N. Giesbrecht, P.M. Pearce, F. Deschler, R.L.Z. Hoye, K.C. Gödel, T. Bein, P. Docampo, S.E. Dutton, M.F.L. De Volder, R.H. Friend. Blue-Green Color Tunable Solution Processable Organolead Chloride–Bromide Mixed Halide Perovskites for Optoelectronic Applications, Nano Letters 15(9) (2015) 6095-6101.

[138] D.N. Congreve, M.C. Weidman, M. Seitz, W. Paritmongkol, N.S. Dahod, W.A. Tisdale. Tunable Light-Emitting Diodes Utilizing Quantum-Confined Layered Perovskite Emitters, ACS Photonics 4(3) (2017) 476-481.

[139] X. Zhang, H. Liu, W. Wang, J. Zhang, B. Xu, K.L. Karen, Y. Zheng, S. Liu, S. Chen, K. Wang, X.W. Sun. Hybrid Perovskite Light-Emitting Diodes Based on Perovskite Nanocrystals with Organic–Inorganic Mixed Cations, Advanced Materials 29(18) (2017) 1606405.

[140] J. Xing, Y. Zhao, M. Askerka, L.N. Quan, X. Gong, W. Zhao, J. Zhao, H. Tan, G. Long, L. Gao, Z. Yang, O. Voznyy, J. Tang, Z.-H. Lu, Q. Xiong, E.H. Sargent. Color-stable highly luminescent sky-blue perovskite light-emitting diodes, Nature Communications 9(1) (2018) 3541.

[141] J. Song, J. Li, X. Li, L. Xu, Y. Dong, H. Zeng. Quantum Dot Light-Emitting Diodes Based on Inorganic Perovskite Cesium Lead Halides (CsPbX3), Advanced Materials 27(44) (2015) 7162-7167.

[142] Y.-H. Kim, C. Wolf, Y.-T. Kim, H. Cho, W. Kwon, S. Do, A. Sadhanala, C.G. Park, S.-W. Rhee, S.H. Im, R.H. Friend, T.-W. Lee. Highly Efficient Light-Emitting Diodes of Colloidal Metal–Halide Perovskite Nanocrystals beyond Quantum Size, ACS Nano 11(7) (2017) 6586-6593.

[143] W. Deng, X. Xu, X. Zhang, Y. Zhang, X. Jin, L. Wang, S.T. Lee, J. Jie. Organometal Halide Perovskite Quantum Dot Light-Emitting Diodes, Advanced Functional Materials 26(26) (2016) 4797-4802.

[144] A. Perumal, S. Shendre, M. Li, Y.K.E. Tay, V.K. Sharma, S. Chen, Z. Wei, Q. Liu, Y. Gao, P.J.S. Buenconsejo, S.T. Tan, C.L. Gan, Q. Xiong, T.C. Sum, H.V. Demir. High brightness formamidinium lead bromide perovskite nanocrystal light emitting devices, Scientific Reports 6 (2016) 36733.

[145] M.F. Aygüler, M.D. Weber, B.M.D. Puscher, D.D. Medina, P. Docampo, R.D. Costa. Light-Emitting Electrochemical Cells Based on Hybrid Lead Halide Perovskite Nanoparticles, The Journal of Physical Chemistry C 119(21) (2015) 12047-12054.

[146] X. Zhang, H. Lin, H. Huang, C. Reckmeier, Y. Zhang, W.C.H. Choy, A.L. Rogach. Enhancing the Brightness of Cesium Lead Halide Perovskite Nanocrystal Based Green Light-Emitting Devices through the Interface Engineering with Perfluorinated Ionomer, Nano Letters 16(2) (2016) 1415-1420.

[147] J. Li, L. Xu, T. Wang, J. Song, J. Chen, J. Xue, Y. Dong, B. Cai, Q. Shan, B. Han, H. Zeng. 50-Fold EQE Improvement up to 6.27% of Solution-Processed All-Inorganic Perovskite CsPbBr3 QLEDs via Surface Ligand Density Control, Advanced Materials 29(5) (2017) 1603885.

[148] G. Nedelcu, L. Protesescu, S. Yakunin, M.I. Bodnarchuk, M.J. Grotevent, M.V. Kovalenko. Fast Anion-Exchange in Highly Luminescent Nanocrystals of Cesium Lead Halide Perovskites (CsPbX3, X = Cl, Br, I), Nano Letters 15(8) (2015) 5635-5640.

[149] T. Chiba, Y. Hayashi, H. Ebe, K. Hoshi, J. Sato, S. Sato, Y.-J. Pu, S. Ohisa, J. Kido. Anion-exchange red perovskite quantum dots with ammonium iodine salts for highly efficient light-emitting devices, Nature Photonics (2018).

[150] Z. Xiao, R.A. Kerner, L. Zhao, N.L. Tran, K.M. Lee, T.-W. Koh, G.D. Scholes, B.P. Rand. Efficient perovskite light-emitting diodes featuring nanometre-sized crystallites, Nature Photonics 11 (2017) 108.

[151] N. Wang, L. Cheng, R. Ge, S. Zhang, Y. Miao, W. Zou, C. Yi, Y. Sun, Y. Cao, R. Yang, Y. Wei, Q. Guo, Y. Ke, M. Yu, Y. Jin, Y. Liu, Q. Ding, D. Di, L. Yang, G. Xing, H. Tian, C. Jin, F. Gao, R.H. Friend, J. Wang, W. Huang. Perovskite light-emitting diodes based on solution-processed self-organized multiple quantum wells, Nature Photonics 10 (2016) 699.

[152] J. Chang, S. Zhang, N. Wang, Y. Sun, Y. Wei, R. Li, C. Yi, J. Wang, W. Huang. Enhanced Performance of Red Perovskite Light-Emitting Diodes through the Dimensional Tailoring of Perovskite Multiple Quantum Wells, The Journal of Physical Chemistry Letters 9(4) (2018) 881-886.

[153] J. Si, Y. Liu, Z. He, H. Du, K. Du, D. Chen, J. Li, M. Xu, H. Tian, H. He, D. Di, C. Lin, Y. Cheng, J. Wang, Y. Jin. Efficient and High-Color-Purity Light-Emitting Diodes Based on In Situ Grown Films of CsPbX3 (X = Br, I) Nanoplates with Controlled Thicknesses, ACS Nano 11(11) (2017) 11100-11107.

[154] C. Qin, T. Matsushima, A.S.D. Sandanayaka, Y. Tsuchiya, C. Adachi. Centrifugal-Coated Quasi-Two-Dimensional Perovskite CsPb2Br5 Films for Efficient and Stable Light-Emitting Diodes, The Journal of Physical Chemistry Letters 8(21) (2017) 5415-5421.

[155] L.N. Quan, Y. Zhao, F.P. García de Arquer, R. Sabatini, G. Walters, O. Voznyy, R. Comin, Y. Li, J.Z. Fan, H. Tan, J. Pan, M. Yuan, O.M. Bakr, Z. Lu, D.H. Kim, E.H. Sargent. Tailoring the Energy Landscape in Quasi-2D Halide Perovskites Enables Efficient Green-Light Emission, Nano Letters 17(6) (2017) 3701-3709.

[156] Z. Chen, C. Zhang, X.-F. Jiang, M. Liu, R. Xia, T. Shi, D. Chen, Q. Xue, Y.-J. Zhao, S. Su, H.-L. Yip, Y. Cao. High-Performance Color-Tunable Perovskite Light Emitting Devices through Structural Modulation from Bulk to Layered Film, Advanced Materials 29(8) (2017) 1603157.

[157] D. Liang, Y. Peng, Y. Fu, M.J. Shearer, J. Zhang, J. Zhai, Y. Zhang, R.J. Hamers, T.L. Andrew, S. Jin. Color-Pure Violet-Light-Emitting Diodes Based on Layered Lead Halide Perovskite Nanoplates, ACS Nano 10(7) (2016) 6897-6904.

[158] P. Vashishtha, M. Ng, S.B. Shivarudraiah, J.E. Halpert. High Efficiency Blue and Green Light-Emitting Diodes Using Ruddlesden–Popper Inorganic Mixed Halide Perovskites with Butylammonium Interlayers, Chemistry of Materials 31(1) (2019) 83-89.

[159] Z. Li, Z. Chen, Y. Yang, Q. Xue, H.-L. Yip, Y. Cao. Modulation of recombination zone position for quasi-two-dimensional blue perovskite light-emitting diodes with efficiency exceeding 5%, Nature Communications 10(1) (2019) 1027.

[160] G. Li, F.W.R. Rivarola, N.J.L.K. Davis, S. Bai, T.C. Jellicoe, F. de la Peña, S. Hou, C. Ducati, F. Gao, R.H. Friend, N.C. Greenham, Z.-K. Tan. Highly Efficient Perovskite

Nanocrystal Light-Emitting Diodes Enabled by a Universal Crosslinking Method, Advanced Materials 28(18) (2016) 3528-3534.

[161] X. Zhang, C. Sun, Y. Zhang, H. Wu, C. Ji, Y. Chuai, P. Wang, S. Wen, C. Zhang, W.W. Yu. Bright Perovskite Nanocrystal Films for Efficient Light-Emitting Devices, The Journal of Physical Chemistry Letters 7(22) (2016) 4602-4610.

[162] X. Zhang, B. Xu, J. Zhang, Y. Gao, Y. Zheng, K. Wang, X.W. Sun. All-Inorganic Perovskite Nanocrystals for High-Efficiency Light Emitting Diodes: Dual-Phase CsPbBr3-CsPb2Br5 Composites, Advanced Functional Materials 26(25) (2016) 4595-4600.

[163] J. Xing, F. Yan, Y. Zhao, S. Chen, H. Yu, Q. Zhang, R. Zeng, H.V. Demir, X. Sun, A. Huan, Q. Xiong. High-Efficiency Light-Emitting Diodes of Organometal Halide Perovskite Amorphous Nanoparticles, ACS Nano 10(7) (2016) 6623-6630.

[164] B. Xu, W. Wang, X. Zhang, W. Cao, D. Wu, S. Liu, H. Dai, S. Chen, K. Wang, X. Sun. Bright and efficient light-emitting diodes based on MA/Cs double cation perovskite nanocrystals, Journal of Materials Chemistry C 5(25) (2017) 6123-6128.

[165] T. Chiba, K. Hoshi, Y.-J. Pu, Y. Takeda, Y. Hayashi, S. Ohisa, S. Kawata, J. Kido. High-Efficiency Perovskite Quantum-Dot Light-Emitting Devices by Effective Washing Process and Interfacial Energy Level Alignment, ACS Applied Materials & Interfaces 9(21) (2017) 18054-18060.

[166] S. Kumar, J. Jagielski, S. Yakunin, P. Rice, Y.-C. Chiu, M. Wang, G. Nedelcu, Y. Kim, S. Lin, E.J.G. Santos, M.V. Kovalenko, C.-J. Shih. Efficient Blue Electroluminescence Using Quantum-Confined Two-Dimensional Perovskites, ACS Nano 10(10) (2016) 9720-9729.

[167] S. Hou, M.K. Gangishetty, Q. Quan, D.N. Congreve. Efficient Blue and White Perovskite Light-Emitting Diodes via Manganese Doping, Joule 2(11) (2018) 2421-2433.

[168] W. Deng, X. Xu, X. Zhang, Y. Zhang, X. Jin, L. Wang, S.-T. Lee, J. Jie. Organometal Halide Perovskite Quantum Dot Light-Emitting Diodes, Advanced Functional Materials 26(26) (2016) 4797-4802.

[169] J. Pan, L.N. Quan, Y. Zhao, W. Peng, B. Murali, S.P. Sarmah, M. Yuan, L. Sinatra, N.M. Alyami, J. Liu, E. Yassitepe, Z. Yang, O. Voznyy, R. Comin, M.N. Hedhili, O.F. Mohammed, Z.H. Lu, D.H. Kim, E.H. Sargent, O.M. Bakr. Highly Efficient Perovskite-Quantum-Dot Light-Emitting Diodes by Surface Engineering, Advanced Materials 28(39) (2016) 8718-8725.

[170] Z. Wang, A. Abbasi, U. Dave, A. De Groote, S. Kumari, B. Kunert, C. Merckling, M. Pantouvaki, Y. Shi, B. Tian. Novel light source integration approaches for silicon photonics, Laser & Photonics Reviews 11(4) (2017) 1700063.

[171] C.Z. Ning. Semiconductor nanolasers, physica status solidi (b) 247(4) (2010) 774-788.

[172] M.H. Huang, S. Mao, H. Feick, H. Yan, Y. Wu, H. Kind, E. Weber, R. Russo, P. Yang. Room-Temperature Ultraviolet Nanowire Nanolasers, Science 292(5523) (2001) 1897-1899.

[173] R. Yan, D. Gargas, P. Yang. Nanowire photonics, Nature Photonics 3 (2009) 569.

[174] B.R. Sutherland, S. Hoogland, M.M. Adachi, P. Kanjanaboos, C.T.O. Wong, J.J. McDowell, J. Xu, O. Voznyy, Z. Ning, A.J. Houtepen, E.H. Sargent. Perovskite Thin Films via Atomic Layer Deposition, Advanced Materials 27(1) (2015) 53-58.

[175] G. Xing, N. Mathews, S. Sun, S.S. Lim, Y.M. Lam, M. Grätzel, S. Mhaisalkar, T.C. Sum. Long-Range Balanced Electron- and Hole-Transport Lengths in Organic-Inorganic $CH_3NH_3PbI_3$, Science 342(6156) (2013) 344-347.

[176] F. Deschler, M. Price, S. Pathak, L.E. Klintberg, D.-D. Jarausch, R. Higler, S. Hüttner, T. Leijtens, S.D. Stranks, H.J. Snaith, M. Atatüre, R.T. Phillips, R.H. Friend. High Photoluminescence Efficiency and Optically Pumped Lasing in Solution-Processed Mixed Halide Perovskite Semiconductors, The Journal of Physical Chemistry Letters 5(8) (2014) 1421-1426.

[177] M. Li, Q. Wei, S.K. Muduli, N. Yantara, Q. Xu, N. Mathews, S.G. Mhaisalkar, G. Xing, T.C. Sum. Enhanced Exciton and Photon Confinement in Ruddlesden–Popper Perovskite Microplatelets for Highly Stable Low-Threshold Polarized Lasing, Advanced Materials 30(23) (2018) 1707235.

[178] R. Chen, T.-T.D. Tran, K.W. Ng, W.S. Ko, L.C. Chuang, F.G. Sedgwick, C. Chang-Hasnain. Nanolasers grown on silicon, Nature Photonics 5 (2011) 170.

[179] S. Yakunin, L. Protesescu, F. Krieg, M.I. Bodnarchuk, G. Nedelcu, M. Humer, G. De Luca, M. Fiebig, W. Heiss, M.V. Kovalenko. Low-threshold amplified spontaneous emission and lasing from colloidal nanocrystals of caesium lead halide perovskites, Nature Communications 6 (2015) 8056.

[180] J.Q. Grim, S. Christodoulou, F. Di Stasio, R. Krahne, R. Cingolani, L. Manna, I. Moreels. Continuous-wave biexciton lasing at room temperature using solution-processed quantum wells, Nature Nanotechnology 9 (2014) 891.

[181] E. Lhuillier, S. Pedetti, S. Ithurria, B. Nadal, H. Heuclin, B. Dubertret. Two-Dimensional Colloidal Metal Chalcogenides Semiconductors: Synthesis, Spectroscopy, and Applications, Accounts of Chemical Research 48(1) (2015) 22-30.

[182] C.A. Leatherdale, W.K. Woo, F.V. Mikulec, M.G. Bawendi. On the Absorption Cross Section of CdSe Nanocrystal Quantum Dots, The Journal of Physical Chemistry B 106(31) (2002) 7619-7622.

[183] L. Protesescu, S. Yakunin, M.I. Bodnarchuk, F. Bertolotti, N. Masciocchi, A. Guagliardi, M.V. Kovalenko. Monodisperse Formamidinium Lead Bromide Nanocrystals with Bright and Stable Green Photoluminescence, Journal of the American Chemical Society 138(43) (2016) 14202-14205.

[184] L. Protesescu, S. Yakunin, S. Kumar, J. Bär, F. Bertolotti, N. Masciocchi, A. Guagliardi, M. Grotevent, I. Shorubalko, M.I. Bodnarchuk, C.-J. Shih, M.V. Kovalenko. Dismantling the "Red Wall" of Colloidal Perovskites: Highly Luminescent Formamidinium and Formamidinium–Cesium Lead Iodide Nanocrystals, ACS Nano 11(3) (2017) 3119-3134.

[185] D. Priante, I. Dursun, M.S. Alias, D. Shi, V.A. Melnikov, T.K. Ng, O.F. Mohammed, O.M. Bakr, B.S. Ooi. The recombination mechanisms leading to amplified spontaneous emission at the true-green wavelength in $CH_3NH_3PbBr_3$ perovskites, Applied Physics Letters 106(8) (2015) 081902.

[186] O. Vybornyi, S. Yakunin, M.V. Kovalenko. Polar-solvent-free colloidal synthesis of highly luminescent alkylammonium lead halide perovskite nanocrystals, Nanoscale 8(12) (2016) 6278-6283.

[187] S.A. Veldhuis, Y.K.E. Tay, A. Bruno, S.S.H. Dintakurti, S. Bhaumik, S.K. Muduli, M. Li, N. Mathews, T.C. Sum, S.G. Mhaisalkar. Benzyl Alcohol-Treated CH3NH3PbBr3 Nanocrystals Exhibiting High Luminescence, Stability, and Ultralow Amplified Spontaneous Emission Thresholds, Nano Letters 17(12) (2017) 7424-7432.

[188] Q. Zhang, R. Su, X. Liu, J. Xing, T.C. Sum, Q. Xiong. High-Quality Whispering-Gallery-Mode Lasing from Cesium Lead Halide Perovskite Nanoplatelets, Advanced Functional Materials 26(34) (2016) 6238-6245.

[189] G. Xing, M.H. Kumar, W.K. Chong, X. Liu, Y. Cai, H. Ding, M. Asta, M. Grätzel, S. Mhaisalkar, N. Mathews, T.C. Sum. Solution-Processed Tin-Based Perovskite for Near-Infrared Lasing, Advanced Materials 28(37) (2016) 8191-8196.

[190] R.L. Milot, G.E. Eperon, T. Green, H.J. Snaith, M.B. Johnston, L.M. Herz. Radiative Monomolecular Recombination Boosts Amplified Spontaneous Emission in HC(NH2)2SnI3 Perovskite Films, The Journal of Physical Chemistry Letters 7(20) (2016) 4178-4184.

[191] C.-Y. Huang, C. Zou, C. Mao, K.L. Corp, Y.-C. Yao, Y.-J. Lee, C.W. Schlenker, A.K.Y. Jen, L.Y. Lin. CsPbBr3 Perovskite Quantum Dot Vertical Cavity Lasers with Low Threshold and High Stability, ACS Photonics 4(9) (2017) 2281-2289.

[192] B. Mayer, D. Rudolph, J. Schnell, S. Morkötter, J. Winnerl, J. Treu, K. Müller, G. Bracher, G. Abstreiter, G. Koblmüller, J.J. Finley. Lasing from individual GaAs-AlGaAs core-shell nanowires up to room temperature, Nature Communications 4 (2013) 2931.

[193] P. Liu, X. He, J. Ren, Q. Liao, J. Yao, H. Fu. Organic–Inorganic Hybrid Perovskite Nanowire Laser Arrays, ACS Nano 11(6) (2017) 5766-5773.

[194] S.W. Eaton, M. Lai, N.A. Gibson, A.B. Wong, L. Dou, J. Ma, L.-W. Wang, S.R. Leone, P. Yang. Lasing in robust cesium lead halide perovskite nanowires, Proceedings of the National Academy of Sciences 113(8) (2016) 1993-1998.

[195] K. Park, J.W. Lee, J.D. Kim, N.S. Han, D.M. Jang, S. Jeong, J. Park, J.K. Song. Light–Matter Interactions in Cesium Lead Halide Perovskite Nanowire Lasers, The Journal of Physical Chemistry Letters 7(18) (2016) 3703-3710.

[196] A.P. Pushkarev, V.I. Korolev, D.I. Markina, F.E. Komissarenko, A. Naujokaitis, A. Drabavičius, V. Pakštas, M. Franckevičius, S.A. Khubezhov, D.A. Sannikov, A.V. Zasedatelev, P.G. Lagoudakis, A.A. Zakhidov, S.V. Makarov. A Few-Minute Synthesis of CsPbBr3 Nanolasers with a High Quality Factor by Spraying at Ambient Conditions, ACS Applied Materials & Interfaces 11(1) (2019) 1040-1048.

[197] Y. Wang, M. Yasar, Z. Luo, S. Zhou, Y. Yu, H. Li, R. Yang, X. Wang, A. Pan, L. Gan, T. Zhai. Temperature Difference Triggering Controlled Growth of All-Inorganic Perovskite Nanowire Arrays in Air, Small 14(41) (2018) 1803010.

[198] H. Zhang, Y. Wu, Q. Liao, Z. Zhang, Y. Liu, Q. Gao, P. Liu, M. Li, J. Yao, H. Fu. A Two-Dimensional Ruddlesden–Popper Perovskite Nanowire Laser Array based on Ultrafast Light-Harvesting Quantum Wells, Angewandte Chemie International Edition 57(26) (2018) 7748-7752.

[199] S. Makarov, A. Furasova, E. Tiguntseva, A. Hemmetter, A. Berestennikov, A. Pushkarev, A. Zakhidov, Y. Kivshar. Halide-Perovskite Resonant Nanophotonics, Advanced Optical Materials 7(1) (2019) 1800784.

[200] Y. Zhang, C.-K. Lim, Z. Dai, G. Yu, J.W. Haus, H. Zhang, P.N. Prasad. Photonics and optoelectronics using nano-structured hybrid perovskite media and their optical cavities, Physics Reports 795 (2019) 1-51.

[201] A.S. Berestennikov, Y. Li, I.V. Iorsh, A.A. Zakhidov, A.L. Rogach, S.V. Makarov. Beyond quantum confinement: excitonic nonlocality in halide perovskite nanoparticles with Mie resonances, Nanoscale 11(14) (2019) 6747-6754.

[202] B. Tang, H. Dong, L. Sun, W. Zheng, Q. Wang, F. Sun, X. Jiang, A. Pan, L. Zhang. Single-Mode Lasers Based on Cesium Lead Halide Perovskite Submicron Spheres, ACS Nano 11(11) (2017) 10681-10688.

[203] E.Y. Tiguntseva, D.G. Baranov, A.P. Pushkarev, B. Munkhbat, F. Komissarenko, M. Franckevičius, A.A. Zakhidov, T. Shegai, Y.S. Kivshar, S.V. Makarov. Tunable Hybrid Fano Resonances in Halide Perovskite Nanoparticles, Nano Letters 18(9) (2018) 5522-5529.

[204] Y. Wang, P. Wang, X. Zhou, C. Li, H. Li, X. Hu, F. Li, X. Liu, M. Li, Y. Song. Solar Cells: Diffraction-Grated Perovskite Induced Highly Efficient Solar Cells through Nanophotonic Light Trapping (Adv. Energy Mater. 12/2018), Advanced Energy Materials 8(12) (2018) 1870052.

[205] J. Mao, W.E.I. Sha, H. Zhang, X. Ren, J. Zhuang, V.A.L. Roy, K.S. Wong, W.C.H. Choy. Novel Direct Nanopatterning Approach to Fabricate Periodically Nanostructured Perovskite for Optoelectronic Applications, Advanced Functional Materials 27(10) (2017) 1606525.

[206] B. Gholipour, G. Adamo, D. Cortecchia, H.N.S. Krishnamoorthy, M.D. Birowosuto, N.I. Zheludev, C. Soci. Organometallic Perovskite Metasurfaces, Advanced Materials 29(9) (2017) 1604268.

[207] H. Deng, G. Weihs, C. Santori, J. Bloch, Y. Yamamoto. Condensation of Semiconductor Microcavity Exciton Polaritons, Science 298(5591) (2002) 199-202.

[208] Q. Shang, S. Zhang, Z. Liu, J. Chen, P. Yang, C. Li, W. Li, Y. Zhang, Q. Xiong, X. Liu, Q. Zhang. Surface Plasmon Enhanced Strong Exciton–Photon Coupling in Hybrid Inorganic–Organic Perovskite Nanowires, Nano Letters 18(6) (2018) 3335-3343.

[209] J. Kasprzak, M. Richard, S. Kundermann, A. Baas, P. Jeambrun, J.M.J. Keeling, F.M. Marchetti, M.H. Szymańska, R. André, J.L. Staehli, V. Savona, P.B. Littlewood, B. Deveaud, L.S. Dang. Bose–Einstein condensation of exciton polaritons, Nature 443 (2006) 409.

[210] D. Bajoni, P. Senellart, E. Wertz, I. Sagnes, A. Miard, A. Lemaître, J. Bloch. Polariton Laser Using Single Micropillar GaAs−GaAlAs Semiconductor Cavities, Physical Review Letters 100(4) (2008) 047401.

[211] P. Bhattacharya, B. Xiao, A. Das, S. Bhowmick, J. Heo. Solid State Electrically Injected Exciton-Polariton Laser, Physical Review Letters 110(20) (2013) 206403.

[212] T. Guillet, M. Mexis, J. Levrat, G. Rossbach, C. Brimont, T. Bretagnon, B. Gil, R. Butté, N. Grandjean, L. Orosz, F. Réveret, J. Leymarie, J. Zúñiga-Pérez, M. Leroux, F. Semond, S. Bouchoule. Polariton lasing in a hybrid bulk ZnO microcavity, Applied Physics Letters 99(16) (2011) 161104.

[213] W. Xie, H. Dong, S. Zhang, L. Sun, W. Zhou, Y. Ling, J. Lu, X. Shen, Z. Chen. Room-Temperature Polariton Parametric Scattering Driven by a One-Dimensional Polariton Condensate, Physical Review Letters 108(16) (2012) 166401.

[214] M. Litinskaya. Exciton polariton kinematic interaction in crystalline organic microcavities, Physical Review B 77(15) (2008) 155325.

[215] R. Su, C. Diederichs, J. Wang, T.C.H. Liew, J. Zhao, S. Liu, W. Xu, Z. Chen, Q. Xiong. Room-Temperature Polariton Lasing in All-Inorganic Perovskite Nanoplatelets, Nano Letters 17(6) (2017) 3982-3988.

[216] Y. Xu, Q. Chen, C. Zhang, R. Wang, H. Wu, X. Zhang, G. Xing, W.W. Yu, X. Wang, Y. Zhang, M. Xiao. Two-Photon-Pumped Perovskite Semiconductor Nanocrystal Lasers, Journal of the American Chemical Society 138(11) (2016) 3761-3768.

[217] Y. Wang, X. Li, X. Zhao, L. Xiao, H. Zeng, H. Sun. Nonlinear Absorption and Low-Threshold Multiphoton Pumped Stimulated Emission from All-Inorganic Perovskite Nanocrystals, Nano Letters 16(1) (2016) 448-453.

[218] B.H. Cumpston, S.P. Ananthavel, S. Barlow, D.L. Dyer, J.E. Ehrlich, L.L. Erskine, A.A. Heikal, S.M. Kuebler, I.Y.S. Lee, D. McCord-Maughon, J. Qin, H. Röckel, M. Rumi, X.-L. Wu, S.R. Marder, J.W. Perry. Two-photon polymerization initiators for three-dimensional optical data storage and microfabrication, Nature 398 (1999) 51.

[219] H. Zhang, J. Fan, K. Wang, J. Li, C. Wang, Y. Nie, T. Jiang, H. Mu, X. Peng, K. Jiang. Highly Sensitive Naphthalene-Based Two-Photon Fluorescent Probe for in Situ Real-Time Bioimaging of Ultratrace Cyclooxygenase-2 in Living Biosystems, Analytical Chemistry 86(18) (2014) 9131-9138.

[220] J.D. Bhawalkar, G.S. He, P.N. Prasad. Nonlinear multiphoton processes in organic and polymeric materials, Reports on Progress in Physics 59(9) (1996) 1041.

[221] V.M. Agranovich, D.M. Basko, G.C.L. Rocca, F. Bassani. Excitons and optical nonlinearities in hybrid organic-inorganic nanostructures, Journal of Physics: Condensed Matter 10(42) (1998) 9369-9400.

[222] G. Walters, B.R. Sutherland, S. Hoogland, D. Shi, R. Comin, D.P. Sellan, O.M. Bakr, E.H. Sargent. Two-Photon Absorption in Organometallic Bromide Perovskites, ACS Nano 9(9) (2015) 9340-9346.

[223] Z. Gu, K. Wang, W. Sun, J. Li, S. Liu, Q. Song, S. Xiao. Two-Photon Pumped CH3NH3PbBr3 Perovskite Microwire Lasers, Advanced Optical Materials 4(3) (2016) 472-479.

[224] M.E. Madjet, G.R. Berdiyorov, F. El-Mellouhi, F.H. Alharbi, A.V. Akimov, S. Kais. Cation Effect on Hot Carrier Cooling in Halide Perovskite Materials, The Journal of Physical Chemistry Letters 8(18) (2017) 4439-4445.

[225] T.R. Hopper, A. Gorodetsky, J.M. Frost, C. Müller, R. Lovrincic, A.A. Bakulin. Ultrafast Intraband Spectroscopy of Hot-Carrier Cooling in Lead-Halide Perovskites, ACS Energy Letters 3(9) (2018) 2199-2205.

[226] Y.-F. Lao, A.G.U. Perera, L.H. Li, S.P. Khanna, E.H. Linfield, H.C. Liu. Tunable hot-carrier photodetection beyond the bandgap spectral limit, Nature Photonics 8 (2014) 412.

[227] M.V. Kovalenko, M. Scheele, D.V. Talapin. Colloidal Nanocrystals with Molecular Metal Chalcogenide Surface Ligands, Science 324(5933) (2009) 1417-1420.

[228] S. Bhaumik, S.A. Veldhuis, Y.F. Ng, M. Li, S.K. Muduli, T.C. Sum, B. Damodaran, S. Mhaisalkar, N. Mathews. Highly stable, luminescent core-shell type methylammonium-

octylammonium lead bromide layered perovskite nanoparticles, Chemical Communications 52(44) (2016) 7118-7121.

[229] K. Leng, I. Abdelwahab, I. Verzhbitskiy, M. Telychko, L. Chu, W. Fu, X. Chi, N. Guo, Z. Chen, Z. Chen, C. Zhang, Q.-H. Xu, J. Lu, M. Chhowalla, G. Eda, K.P. Loh. Molecularly thin two-dimensional hybrid perovskites with tunable optoelectronic properties due to reversible surface relaxation, Nature Materials 17(10) (2018) 908-914.

[230] W. Niu, A. Eiden, G.V. Prakash, J.J. Baumberg. Exfoliation of self-assembled 2D organic-inorganic perovskite semiconductors, Applied Physics Letters 104(17) (2014) 171111.

[231] V.A. Hintermayr, A.F. Richter, F. Ehrat, M. Döblinger, W. Vanderlinden, J.A. Sichert, Y. Tong, L. Polavarapu, J. Feldmann, A.S. Urban. Tuning the Optical Properties of Perovskite Nanoplatelets through Composition and Thickness by Ligand-Assisted Exfoliation, Advanced Materials 28(43) (2016) 9478-9485.

[232] L. Dou, A.B. Wong, Y. Yu, M. Lai, N. Kornienko, S.W. Eaton, A. Fu, C.G. Bischak, J. Ma, T. Ding, N.S. Ginsberg, L.-W. Wang, A.P. Alivisatos, P. Yang. Atomically thin two-dimensional organic-inorganic hybrid perovskites, Science 349(6255) (2015) 1518-1521.